


Revisiting CP violation in $D \rightarrow PP$ and VP decays

Hai-Yang Cheng 

Institute of Physics, Academia Sinica, Taipei, Taiwan 11529, Republic of China

Cheng-Wei Chiang 

Department of Physics, National Taiwan University, Taipei, Taiwan 10617, Republic of China



(Received 17 September 2019; published 11 November 2019)

Direct CP violation in the hadronic charm decays provides a good testing ground for the Kobayashi-Maskawa mechanism in the Standard Model. Any significant deviations from the expectation would be indirect evidence of physics beyond the Standard Model. In view of improved measurements from LHCb and BESIII experiments, we reanalyze the Cabibbo-favored $D \rightarrow PP$ and VP decays in the topological diagram approach. By assuming certain SU(3)-breaking effects in the tree-type amplitudes, we make predictions for both branching fractions and CP asymmetries of the singly Cabibbo-suppressed decay modes. While the color-allowed and -suppressed amplitudes are preferred to scale by the factor dictated by factorization in the PP modes, no such scaling is required in the VP modes. The W -exchange amplitudes are found to change by 10% to 50% and depend on whether the $d\bar{d}$ or $s\bar{s}$ pair directly emerges from W -exchange. The predictions of branching fractions are generally improved after these SU(3) symmetry breaking effects are taken into account. We show in detail how the tree-type, QCD-penguin, and weak penguin-annihilation diagrams contribute and modify CP asymmetry predictions. Future measurements of sufficiently many direct CP asymmetries will be very useful in removing a discrete ambiguity in the strong phases as well as discriminating among different theory approaches. In particular, we predict $a_{CP}(K^+K^-) - a_{CP}(\pi^+\pi^-) = (-1.14 \pm 0.26) \times 10^{-3}$ or $(-1.25 \pm 0.25) \times 10^{-3}$, consistent with the latest data, and $a_{CP}(K^+K^{*-}) - a_{CP}(\pi^+\rho^-) = (-1.52 \pm 0.43) \times 10^{-3}$, an attractive and measurable observable in the near future. Moreover, we observe that such CP asymmetry differences are dominated by long-distance penguin-exchange through final-state rescattering.

DOI: [10.1103/PhysRevD.100.093002](https://doi.org/10.1103/PhysRevD.100.093002)

I. INTRODUCTION

Based on 0.62 fb^{-1} of 2011 data, in 2012 the LHCb collaboration has reported a result of a nonzero value for the difference between the time-integrated CP asymmetries of the decays $D^0 \rightarrow K^+K^-$ and $D^0 \rightarrow \pi^+\pi^-$ [1]:

$$\begin{aligned} \Delta A_{CP} &\equiv a_{CP}(K^+K^-) - a_{CP}(\pi^+\pi^-) \\ &= -(0.82 \pm 0.21 \pm 0.11)\% \quad (\text{LHCb 2012}). \end{aligned} \quad (1)$$

The time-integrated asymmetry can be further decomposed into a direct CP asymmetry a_{CP}^{dir} and a mixing-induced indirect CP asymmetry a_{CP}^{ind}

$$a_{CP}(f) = a_{CP}^{\text{dir}}(f) \left(1 + \frac{\langle t \rangle}{\tau} y_{CP} \right) + \frac{\langle t \rangle}{\tau} a_{CP}^{\text{ind}}, \quad (2)$$

where $\langle t \rangle$ is the average decay time in the sample, τ is the D^0 lifetime and y_{CP} is the deviation from unity of the ratio of the effective lifetimes of D^0 meson decays to flavor-specific and CP -even final states. To a good approximation, a_{CP}^{ind} is independent of the decay mode. Hence,

$$\Delta A_{CP} = \Delta a_{CP}^{\text{dir}} \left(1 + \frac{\langle t \rangle}{\tau} y_{CP} \right) + \frac{\Delta \langle t \rangle}{\tau} a_{CP}^{\text{ind}}. \quad (3)$$

Based on the LHCb averages of y_{CP} and a_{CP}^{ind} , it is known that ΔA_{CP} is primarily sensitive to direct CP violation.

Since $\Delta a_{CP}^{\text{dir}}$ in the Standard Model (SM) is naively expected to be at most of order 1×10^{-3} , many new physics models [2–15] had been proposed to explain the measurement of large ΔA_{CP} , although it was also argued in [16–23] that large CP asymmetries in singly Cabibbo-suppressed (SCS) D decays were allowed in the SM due to some nonperturbative effects or unexpected strong dynamics and the measured $\Delta a_{CP}^{\text{dir}}$ could be accommodated or marginally achieved.

Published by the American Physical Society under the terms of the [Creative Commons Attribution 4.0 International license](https://creativecommons.org/licenses/by/4.0/). Further distribution of this work must maintain attribution to the author(s) and the published article's title, journal citation, and DOI. Funded by SCOAP³.

On the experimental side, the large ΔA_{CP} observed by LHCb in 2011 was subsequently confirmed by CDF [24] and by Belle [25]. However, the effects disappeared in the muon-tag LHCb analyses in 2013 and 2014 [26,27] and were not seen in the subsequent pion-tag analysis in 2016 [28]. Finally, in this year LHCb announced the measurements based on pion and muon tagged analyses [29]. Combining these with previous LHCb results in 2014 and 2016 leads to [29]

$$\Delta A_{CP} = (-1.54 \pm 0.29) \times 10^{-3}, \quad (\text{LHCb 2019}), \quad (4)$$

which yields $\Delta a_{CP}^{\text{dir}} = (-1.56 \pm 0.29) \times 10^{-3}$. This is the first observation of CP violation in the charm sector.

It is most important to explore whether the first observation of CP violation in the charm sector (4) is consistent with the Standard Model or not.¹ A common argument against the SM interpretation of Eq. (4) goes as follows. Consider the tree T and penguin P contributions to $D^0 \rightarrow K^+ K^-$ and $D^0 \rightarrow \pi^+ \pi^-$. A simplified expression of the CP asymmetry difference between them is given by [for a complete expression of $\Delta a_{CP}^{\text{dir}}$, see Eq. (28) below]

$$\Delta a_{CP}^{\text{dir}} \approx -1.3 \times 10^{-3} \left(\left| \frac{P}{T} \right|_{KK} \sin \theta_{KK} + \left| \frac{P}{T} \right|_{\pi\pi} \sin \theta_{\pi\pi} \right), \quad (5)$$

where θ_{KK} is the strong phase of $(P/T)_{KK}$ and likewise for $\theta_{\pi\pi}$. Since $|P/T|$ is naively expected to be of order $(\alpha_s(\mu_c)/\pi) \sim \mathcal{O}(0.1)$, it appears that $\Delta a_{CP}^{\text{dir}}$ is most likely of order 10^{-4} even if the strong phases are allowed to be close to 90° . Indeed, using the results of $|P/T|$ obtained from light-cone sum rules, the authors of [35] claimed an upper bound in the SM, $|\Delta A_{CP}^{\text{SM}}| \leq (2.0 \pm 0.3) \times 10^{-4}$. The notion that this would imply new physics was reinforced by a recent similar analysis [31].

In 2012, we have studied direct CP violation in charmed meson decays based on the topological diagram approach for tree amplitudes and QCD factorization for penguin amplitudes [36,37]. We have pointed out the importance of a resonantlike final-state rescattering which has the same topology as the QCD-penguin exchange topological graph. Hence, penguin annihilation receives sizable long-distance contributions from final-state interactions. We have shown that $\Delta a_{CP}^{\text{dir}}$ arises mainly from long-distance weak penguin annihilation. Moreover, we predicted that $\Delta a_{CP}^{\text{dir}}$ is about $(-0.139 \pm 0.004)\%$ and $(-0.151 \pm 0.004)\%$ for the two solutions of W -exchange amplitudes [37]. Those were the main predictions among others made in 2012. Since the world average during that time was $\Delta a_{CP}^{\text{dir}} = (-0.645 \pm 0.180)\%$ [38], we concluded that if this CP asymmetry

difference continues to be large with more statistics in the future, it will be clear evidence of physics beyond the Standard Model in the charm sector. Nowadays, we know that the LHCb new measurement almost coincides with our second solution. This implies that one does not need new physics at all to understand the first observation of $\Delta a_{CP}^{\text{dir}}$ by LHCb.²

The purpose of this work is twofold. First, we would like to improve the analysis of CP asymmetries in $D \rightarrow PP$ decays. For example, it is well known that the penguin-exchange amplitude PE and the penguin-annihilation one PA evaluated in the approach of QCD factorization is subject to the end-point divergence. We need to address this issue. Also in our previous study of the long-distance contribution to PE , we did not consider the uncertainties connected with final-state rescattering [37]. This will be improved in this work. Second, although we have studied CP asymmetries in $D \rightarrow VP$ decays before in [36], we focused only to the neutral charmed meson ones. Owing to the lack of information on W -annihilation amplitudes, no prediction was attempted for $D^+ \rightarrow VP$ and $D_s^+ \rightarrow VP$ decays. Thanks to the *BABAR* measurement of $D_s^+ \rightarrow \pi^+ \rho^0$ [40], the amplitudes $A_{V,P}$ can be extracted for the first time in [41]. Consequently, in this work we are able to complete the analysis of CP violation in the VP sector.

The layout of the present paper is as follows. After a brief review of the diagrammatic approach, we study various mechanisms responsible for the large $SU(3)$ violation in the branching fraction ratio of $D^0 \rightarrow K^+ K^-$ to $D^0 \rightarrow \pi^+ \pi^-$ and fix the $SU(3)$ breaking effects in weak annihilation amplitudes in Sec. II. Penguin amplitudes are studied in the framework of QCD factorization as illustrated in Sec. II C. We then discuss direct CP violation in SCS $D \rightarrow PP$ decays in Sec. III and compare our results with other works in the literature. Section IV is devoted to $D \rightarrow VP$ decays and their direct CP asymmetries. Finally, in Sec. V we come to our conclusions.

II. $D \rightarrow PP$ DECAYS

It is known that a reliable theoretical description of the underlying mechanism for exclusive hadronic D decays based on QCD is still not yet available as the mass of the charm quark, being about 1.3 GeV, is not heavy enough to allow for a sensible heavy quark expansion. It has been established sometime ago that a more suitable framework for the analysis of hadronic charmed meson decays is the so-called topological diagram approach [42–44]. In this diagrammatic scenario, the topological diagrams can be classified into three distinct groups (see Fig. 1 of [36]). The first two of them (see [45] for details) are:

¹There were a few theory papers [30–34] after the 2019 LHCb measurement.

²A similar result of $\Delta a_{CP}^{\text{dir}}$ based on a variant of the diagrammatic approach was obtained in [39].

- (1) Tree and penguin amplitudes: color-allowed tree amplitude T ; color-suppressed tree amplitude C ; QCD-penguin amplitude P ; singlet QCD-penguin amplitude S involving flavor SU(3)-singlet mesons; color-favored electroweak-penguin (EW-penguin) amplitude P_{EW} ; and color-suppressed EW-penguin amplitude P_{EW}^C .
- (2) Weak annihilation amplitudes: W -exchange amplitude E ; W -annihilation amplitude A ; QCD-penguin exchange amplitude PE ; QCD-penguin annihilation amplitude PA ; EW-penguin exchange amplitude PE_{EW} ; and EW-penguin annihilation amplitude PA_{EW} .

In this approach, the topological diagrams are classified according to the topologies in the flavor flow of weak decay diagrams, with all strong interaction effects included implicitly in all possible ways. Therefore, analyses of topological graphs can provide valuable information on final-state interactions.

A. Topological amplitudes

The topological amplitudes T, C, E, A are extracted from the Cabibbo-favored (CF) $D \rightarrow PP$ decays [46] to be (in units of 10^{-6} GeV)

$$\begin{aligned} T &= 3.113 \pm 0.011, & C &= (2.767 \pm 0.029)e^{-i(151.3 \pm 0.3)^\circ}, \\ E &= (1.48 \pm 0.04)e^{i(120.9 \pm 0.4)^\circ}, & A &= (0.55 \pm 0.03)e^{i(23_{-10}^{+7})^\circ} \end{aligned} \quad (6)$$

for $\phi = 43.5^\circ$ [47], where ϕ is the $\eta - \eta'$ mixing angle defined in the flavor basis

$$\begin{pmatrix} \eta \\ \eta' \end{pmatrix} = \begin{pmatrix} \cos \phi & -\sin \phi \\ \sin \phi & \cos \phi \end{pmatrix} \begin{pmatrix} \eta_q \\ \eta_s \end{pmatrix}, \quad (7)$$

with $\eta_q = \frac{1}{\sqrt{2}}(u\bar{u} + d\bar{d})$ and $\eta_s = s\bar{s}$. The fitted χ^2 value is 0.135 per degree of freedom. Comparing with the amplitudes obtained in a previous fit in [48]

$$\begin{aligned} T &= 3.14 \pm 0.06, & C &= (2.61 \pm 0.08)e^{-i(152 \pm 1)^\circ}, \\ E &= (1.53_{-0.08}^{+0.07})e^{i(122 \pm 2)^\circ}, & A &= (0.39_{-0.09}^{+0.13})e^{i(31_{-33}^{+20})^\circ} \end{aligned} \quad (8)$$

we see that the errors in T, C, E and A are substantially reduced, especially for the annihilation amplitude A , thanks to the improved data precision from 2019 PDG [46].

We note in passing that since we will only fit to the observed branching fractions, the results will be the same if all the strong phases are subject to a simultaneous sign flip. Throughout this paper, we only present one of them. Presumably, such a degeneracy in strong phases can be resolved by measurements of sufficiently many CP asymmetries.

One of the most important moral lessons we have learnt from this approach is that all the topological amplitudes

except the tree amplitude T given in Eq. (6) are dominated by nonfactorizable long-distance effects. For example, in the naive factorization approach, the topological amplitudes T and C in CF $D \rightarrow \bar{K}\pi$ decays have the expressions

$$\begin{aligned} T &= \frac{G_F}{\sqrt{2}} a_1(\bar{K}\pi) f_\pi (m_D^2 - m_K^2) F_0^{DK}(m_\pi^2), \\ C &= \frac{G_F}{\sqrt{2}} a_2(\bar{K}\pi) f_K (m_D^2 - m_\pi^2) F_0^{D\pi}(m_K^2), \end{aligned} \quad (9)$$

with $a_1 = c_1 + c_2/3$ and $a_2 = c_2 + c_1/3$. It turns out that $a_1(\bar{K}\pi) \approx 1.22$ and $a_2(\bar{K}\pi) \approx 0.82e^{-i(151)^\circ}$ [48] extracted from the experimental values of T and C given in Eq. (6) and the phenomenological model for the D to K and π transition form factors. Since $c_1(m_c) \approx 1.274$ and $c_2(m_c) \approx -0.529$, it is evident that $a_1 = c_1 + c_2/3 \approx 1.09$ is close to $a_1(\bar{K}\pi)$, while $a_2 = c_2 + c_1/3 \approx -0.11$ expected from naive factorization is far off from $a_2(\bar{K}\pi)$, including its size and phase. This implies that the short-distance contribution to C is very suppressed relative to the long-distance one. In the topological approach, the long-distance color-suppressed C is induced from the color-allowed T through final-state rescattering with quark exchange. The nontrivial relative phase between C and T indicates that final-state interactions (FSIs) via quark exchange are responsible for this.

Likewise, short-distance weak annihilation diagrams are helicity suppressed, whereas data imply large sizes of them. This is because they receive large $1/m_c$ power corrections from FSIs and large nonfactorizable contributions for a_2 . For example, the topological amplitude E receives contributions from the tree amplitude T via final-state rescattering with nearby resonance effects. The large magnitude and phase of weak annihilation can be quantitatively and qualitatively understood as elaborated in Refs. [49,50].

As emphasized in [36], one of the great merits of the topological approach is that the magnitude and the relative strong phase of each individual topological tree amplitude in charm decays can be extracted from the data. Consequently, direct CP asymmetries in charmed meson decays induced at the tree level can be reliably estimated as we shall discuss in Sec. III A.

B. Flavor SU(3) symmetry breaking

Using the topological amplitudes in Eq. (6) extracted from the CF modes, we can predict the rates for the SCS decays (see the second column of Table II below). It is known that there exists significant SU(3) breaking in some of the SCS modes from the flavor SU(3) symmetry limit. For example, the rate of $D^0 \rightarrow K^+K^-$ is larger than that of $D^0 \rightarrow \pi^+\pi^-$ by a factor of 2.8 [46], while the magnitudes of their decay amplitudes should be the same in the SU(3) limit. This is a long-standing puzzle since SU(3) symmetry is expected to be broken roughly at the level of 30%.

Also, the decay $D^0 \rightarrow K^0 \bar{K}^0$ is almost prohibited in the SU(3) symmetry limit, but the measured branching fraction is of the same order of magnitude as that of $D^0 \rightarrow \pi^0 \pi^0$.

Since SU(3) breaking effects in $D \rightarrow PP$ decays have been discussed in detail in [37], in this section we will recapitulate the main points and update some of the results.

As stressed in [51], a most natural way of solving the above-mentioned long-standing puzzles is that the overall seemingly large SU(3) symmetry violation arises from the accumulation of several small and nominal SU(3) breaking effects in the tree amplitudes T and E . We will illustrate this point. Following [21], we write

$$\begin{aligned} A(D^0 \rightarrow \pi^+ \pi^-) &= \lambda_d(T + E + P_d + PE_d + PA_d)_{\pi\pi} \\ &\quad + \lambda_s(P_s + PE_s + PA_s)_{\pi\pi} \\ &= \frac{1}{2}(\lambda_d - \lambda_s)(T + E + \Delta P)_{\pi\pi} \\ &\quad - \frac{1}{2}\lambda_b(T + E + \Sigma P)_{\pi\pi}, \end{aligned} \quad (10)$$

where $\lambda_p \equiv V_{cp}^* V_{up}$ ($p = d, s, b$), the subscript refers to the quark involved in the associated penguin loop, and

$$\begin{aligned} \Delta P &\equiv (P_d + PE_d + PA_d) - (P_s + PE_s + PA_s), \\ \Sigma P &\equiv (P_d + PE_d + PA_d) + (P_s + PE_s + PA_s). \end{aligned} \quad (11)$$

Likewise,

$$\begin{aligned} A(D^0 \rightarrow K^+ K^-) &= \lambda_d(P_d + PE_d + PA_d)_{KK} \\ &\quad + \lambda_s(T + E + P_s + PE_s + PA_s)_{KK} \\ &= \frac{1}{2}(\lambda_s - \lambda_d)(T + E - \Delta P)_{KK} \\ &\quad - \frac{1}{2}\lambda_b(T + E + \Sigma P)_{KK}. \end{aligned} \quad (12)$$

As far as the rate is concerned, we can neglect the term with the coefficient λ_b which is much smaller than $(\lambda_d - \lambda_s)$. SU(3)-breaking effects in the tree amplitudes T can be estimated in the factorization approach as

$$\frac{T_{KK}}{T} = \frac{f_K F_0^{DK}(m_K^2)}{f_\pi F_0^{DK}(m_\pi^2)}, \quad \frac{T_{\pi\pi}}{T} = \frac{m_D^2 - m_\pi^2}{m_D^2 - m_K^2} \frac{F_0^{D\pi}(m_\pi^2)}{F_0^{DK}(m_\pi^2)}, \quad (13)$$

where T is the tree amplitude in CF $D \rightarrow \bar{K}\pi$ decays given in Eq. (9). Using the form-factor q^2 dependence determined experimentally from Ref. [52], we find

$$|T_{KK}/T| = 1.269, \quad |T_{\pi\pi}/T| = 0.964. \quad (14)$$

SU(3) symmetry should be also broken in the W -exchange amplitudes. This can be seen from the

observation of the decay $D^0 \rightarrow K^0 \bar{K}^0$ whose decay amplitude is given by

$$A(D^0 \rightarrow K^0 \bar{K}^0) = \lambda_d(E_d + 2PA_d) + \lambda_s(E_s + 2PA_s), \quad (15)$$

with E_q referring to the W -exchange amplitude associated with $c\bar{u} \rightarrow q\bar{q}$ ($q = d, s$). In the SU(3) limit, the decay amplitude is proportional to λ_b and hence its rate is negligibly small, while experimentally $\mathcal{B}(D^0 \rightarrow K^0 \bar{K}^0) = (0.282 \pm 0.010) \times 10^{-3}$ [46]. This implies sizable SU(3) symmetry violation in the W -exchange and QCD-penguin annihilation amplitudes. Neglecting PA and λ_b terms and assuming that the T and E amplitudes are responsible for the SU(3) symmetry breaking, we can fix the SU(3) breaking effects in the W -exchange amplitudes from the following four D^0 decay modes: $K^+ K^-$, $\pi^+ \pi^-$, $\pi^0 \pi^0$ and $K^0 \bar{K}^0$ [37]. A fit to the data yields two possible solutions:

$$\begin{aligned} \text{I: } E_d &= 1.10e^{i15.1^\circ} E, & E_s &= 0.62e^{-i19.7^\circ} E; \\ \text{II: } E_d &= 1.10e^{i15.1^\circ} E, & E_s &= 1.42e^{-i13.5^\circ} E. \end{aligned} \quad (16)$$

The corresponding χ^2 vanishes as these two solutions can be obtained exactly.

If the SU(3)-breaking effects in the T and C topologies are ignored, we find that χ^2 will become very large, of order 340. This is understandable because the large rate disparity between $K^+ K^-$ and $\pi^+ \pi^-$ cannot rely solely on the nominal SU(3) breaking in the tree or W -exchange amplitudes. When considering SU(3)-breaking effects in T , we find that $\mathcal{B}(D^0 \rightarrow \pi^+ \pi^-)$ is reduced slightly from 2.27 (in units of 10^{-3}) to 2.11, while $\mathcal{B}(D^0 \rightarrow K^+ K^-)$ is increased substantially from 1.91 to 3.15 [see Eq. (14)]. When E is replaced by $E_d = 1.10e^{i15^\circ} E$ in the amplitude of $D^0 \rightarrow \pi^+ \pi^-$, the magnitude of $(0.96T + E_d)$ in $A(D^0 \rightarrow \pi^+ \pi^-)$ becomes smaller than that of $(0.96T + E)$ as the phase of E is about 121° , so that $\mathcal{B}(D^0 \rightarrow \pi^+ \pi^-)$ is decreased further from 2.11 to 1.47. Likewise, with E being replaced by $E_s = 0.62e^{-i20^\circ} E$ or $E_s = 1.42e^{-i14^\circ} E$ in the amplitude of $D^0 \rightarrow K^+ K^-$, the magnitude of $(1.27T + E_s)$ is enhanced relative to $(1.27T + E)$. It follows that $\mathcal{B}(D^0 \rightarrow K^+ K^-)$ is increased further from 3.15 to 4.03 or 4.05. This shows that the seemingly large SU(3) symmetry violation in $\Gamma(D^0 \rightarrow K^+ K^-)$ and $\Gamma(D^0 \rightarrow \pi^+ \pi^-)$ simply follows from the accumulation of several smaller and nominal SU(3) breaking effects in the tree amplitudes T and E .

At the hadron level, flavor SU(3) breaking due to the strange and light quark differences will manifest in the decay constants, form factors, wave functions and hadron masses, etc. That is how we evaluate the SU(3)-breaking effect in the T amplitude via Eq. (13). Since the W -exchange is governed by long-distance effects, we do not know how to estimate its SU(3) symmetry violation.

TABLE I. Topological amplitudes for singly Cabibbo-suppressed decays of charmed mesons to two pseudoscalar mesons where flavor SU(3) symmetry breaking effects are included. Summation over $p = d, s$ is understood.

	Mode	Representation
D^0	$\pi^+\pi^-$	$\lambda_d(0.96T + E_d) + \lambda_p(P_p + PE_p + PA_p)$
	$\pi^0\pi^0$	$\frac{1}{\sqrt{2}}\lambda_d(-0.78C + E_d) + \frac{1}{\sqrt{2}}\lambda_p(P_p + PE_p + PA_p)$
	$\pi^0\eta$	$-\lambda_d(E_d)\cos\phi - \frac{1}{\sqrt{2}}\lambda_s(1.28C)\sin\phi + \lambda_p(P_p + PE_p)\cos\phi$
	$\pi^0\eta'$	$-\lambda_d(E_d)\sin\phi + \frac{1}{\sqrt{2}}\lambda_s(1.28C)\cos\phi + \lambda_p(P_p + PE_p)\sin\phi$
	$\eta\eta$	$\frac{1}{\sqrt{2}}\lambda_d(0.78C + E_d)\cos^2\phi + \lambda_s(-\frac{1}{2}1.08C\sin 2\phi + \sqrt{2}E_s\sin^2\phi) + \frac{1}{\sqrt{2}}\lambda_p(P_p + PE_p + PA_p)\cos^2\phi$
	$\eta\eta'$	$\frac{1}{2}\lambda_d(0.78C + E_d)\sin 2\phi + \lambda_s(\frac{1}{\sqrt{2}}1.08C\cos 2\phi - E_s\sin 2\phi) + \frac{1}{2}\lambda_p(P_p + PE_p + PA_p)\sin 2\phi$
	K^+K^-	$\lambda_s(1.27T + E_s) + \lambda_p(P_p + PE_p + PA_p)$
	$K^0\bar{K}^0$	$\lambda_d(E_d) + \lambda_s(E_s) + 2\lambda_p(PA_p)$
D^+	$\pi^+\pi^0$	$\frac{1}{\sqrt{2}}\lambda_d(0.97T + 0.78C)$
	$\pi^+\eta$	$\frac{1}{\sqrt{2}}\lambda_d(0.82T + 0.93C + 1.19A)\cos\phi - \lambda_s(1.28C)\sin\phi + \sqrt{2}\lambda_p(P_p + PE_p)\cos\phi$
	$\pi^+\eta'$	$\frac{1}{\sqrt{2}}\lambda_d(0.82T + 0.93C + 1.61A)\sin\phi + \lambda_s(1.28C)\cos\phi + \sqrt{2}\lambda_p(P_p + PE_p)\sin\phi$
	$K^+\bar{K}^0$	$\lambda_d(0.85A) + \lambda_s(1.28T) + \lambda_p(P_p + PE_p)$
D_s^+	π^+K^0	$\lambda_d(1.00T) + \lambda_s(0.84A) + \lambda_p(P_p + PE_p)$
	π^0K^+	$\frac{1}{\sqrt{2}}[-\lambda_d(0.81C) + \lambda_s(0.84A) + \lambda_p(P_p + PE_p)]$
	$K^+\eta$	$\frac{1}{\sqrt{2}}\lambda_p[0.92C\delta_{pd} + 1.14A\delta_{ps} + P_p + PE_p]\cos\phi - \lambda_p[(1.31T + 1.27C + 1.14A)\delta_{ps} + P_p + PE_p]\sin\phi$
	$K^+\eta'$	$\frac{1}{\sqrt{2}}\lambda_p[0.92C\delta_{pd} + 1.14A\delta_{ps} + P_p + PE_p]\sin\phi + \lambda_p[(1.31T + 1.27C + 1.14A)\delta_{ps} + P_p + PE_p]\cos\phi$

Hence, we rely on the four modes: K^+K^- , $\pi^+\pi^-$, $\pi^0\pi^0$ and $K^0\bar{K}^0$ to extract E_d and E_s .

Different mechanisms have been proposed in the literature for explaining the large rate difference between $D^0 \rightarrow \pi^+\pi^-$ and $D^0 \rightarrow K^+K^-$. For example, it has been argued that ΔP dominated by the difference of s - and d -quark penguin contractions of 4-quark tree operators is responsible for the large SU(3) breaking in K^+K^- and $\pi^+\pi^-$ modes [21]. However, this requires that $|\Delta P/T| \sim 0.5$. This mechanism demands a large penguin which is comparable or even larger than T . Moreover, it requires a large difference between s - and d -quark penguin contractions. In Sec. III B, we shall see that $|\Delta P/T|$ is estimated to be of order 0.01 for the short-distance ΔP . Because of the smallness of ΔP , we need to rely on SU(3) violation in both T and E amplitudes to explain the large disparity in the rates of $D^0 \rightarrow K^+K^-$ and $\pi^+\pi^-$.

Another scenario in which the dominant source of SU(3) breaking lies in final-state interactions was advocated recently in [53]. To fit the data, several large strong phases such as δ_0 , δ_1 and $\delta_{1/2}$ from final-state interactions are needed [53]. They deviate substantially from the SU(3) limit, namely, $\delta_0 = \delta_1 = \delta_{1/2}$.

SU(3) breaking effects in the topological amplitudes for SCS $D \rightarrow PP$ decays are summarized in Table I. For simplicity, flavor-singlet QCD penguin, flavor-singlet weak annihilation and electroweak penguin annihilation amplitudes have been neglected in subsequent numerical analyses. The reader is referred to Refs. [37,48] in which we have illustrated SU(3) breaking effects in some selective SCS

modes. The predicted and measured branching fractions are given in Table II.³ While the agreement with experiment is improved for most of the SCS modes after taking into account SU(3) breaking effects in decay amplitudes, there are a few exceptions. For example, the predicted rate for $D^0 \rightarrow \pi^0\eta^{(\prime)}$ becomes slightly worse compared to the prediction based on SU(3) symmetry even though $D^+ \rightarrow \pi^+\eta^{(\prime)}$ works better in the presence of SU(3) breaking.

C. Penguin amplitudes in QCD factorization

Although the topological tree amplitudes T , C , E and A for hadronic D decays can be extracted from the data, information on penguin amplitudes (QCD penguin, penguin annihilation, etc.) is still needed in order to estimate CP violation in the SCS decays. To calculate the penguin contributions, we start from the short-distance effective Hamiltonian

$$\mathcal{H}_{\text{eff}} = \frac{G_F}{\sqrt{2}} \left[\sum_{p=d,s} \lambda_p (c_1 O_1^p + c_2 O_2^p + c_{8g} O_{8g}) - \lambda_b \sum_{i=3}^6 c_i O_i \right], \quad (19)$$

³Throughout this paper, predictions are made by sampling 10^4 points in the parameter space, assuming that each of the parameters has a Gaussian distribution with the corresponding central value and symmetrized standard deviation. Then the predicted values are the mean and standard deviation of data computed using the 10^4 points.

TABLE II. Branching fractions (in units of 10^{-3}) of singly Cabibbo-suppressed $D \rightarrow PP$ decays. The column denoted by $\mathcal{B}_{\text{SU}(3)}$ shows the predictions based on our best-fitted results in Eq. (6) with exact flavor SU(3) symmetry, while SU(3) symmetry breaking effects are taken into account in the column denoted by $\mathcal{B}_{\text{SU}(3)\text{-breaking}}$. The first (second) entry in $D^0 \rightarrow \eta\eta, \eta\eta', K^+K^-$ and $K^0\bar{K}^0$ modes is for Solution I (II) of E_d and E_s in Eq. (16). Experimental results of branching fractions are taken from PDG [46].

Decay Mode	$\mathcal{B}_{\text{SU}(3)}$	$\mathcal{B}_{\text{SU}(3)\text{-breaking}}$	$\mathcal{B}_{\text{expt}}$
$D^0 \rightarrow \pi^+\pi^-$	2.28 ± 0.02	1.47 ± 0.02	1.455 ± 0.024
$D^0 \rightarrow \pi^0\pi^0$	1.50 ± 0.03	0.82 ± 0.02	0.826 ± 0.025
$D^0 \rightarrow \pi^0\eta$	0.83 ± 0.02	0.92 ± 0.02	0.63 ± 0.06
$D^0 \rightarrow \pi^0\eta'$	0.75 ± 0.02	1.36 ± 0.03	0.92 ± 0.10
$D^0 \rightarrow \eta\eta$	1.52 ± 0.03	1.82 ± 0.04	2.11 ± 0.19
	1.52 ± 0.03	2.11 ± 0.04	
$D^0 \rightarrow \eta\eta'$	1.28 ± 0.05	0.69 ± 0.03	1.01 ± 0.19
	1.28 ± 0.05	1.63 ± 0.08	
$D^0 \rightarrow K^+K^-$	1.91 ± 0.02	4.03 ± 0.03	4.08 ± 0.06
	1.91 ± 0.02	4.05 ± 0.05	
$D^0 \rightarrow K_S K_S$	0	0.141 ± 0.007	0.141 ± 0.005
	0	0.141 ± 0.007	
$D^+ \rightarrow \pi^+\pi^0$	0.89 ± 0.02	0.93 ± 0.02	1.247 ± 0.033
$D^+ \rightarrow \pi^+\eta$	1.90 ± 0.16	4.08 ± 0.16	3.77 ± 0.09
$D^+ \rightarrow \pi^+\eta'$	4.21 ± 0.12	4.69 ± 0.08	4.97 ± 0.19
$D^+ \rightarrow K^+K_S$	2.29 ± 0.09	4.25 ± 0.10	3.04 ± 0.09
$D_s^+ \rightarrow \pi^+K_S$	1.20 ± 0.04	1.27 ± 0.04	1.22 ± 0.06
$D_s^+ \rightarrow \pi^0K^+$	0.86 ± 0.04	0.56 ± 0.02	0.63 ± 0.21
$D_s^+ \rightarrow K^+\eta$	0.91 ± 0.03	0.86 ± 0.03	1.77 ± 0.35
$D_s^+ \rightarrow K^+\eta'$	1.23 ± 0.06	1.49 ± 0.08	1.8 ± 0.6

where

$$\begin{aligned}
O_1^p &= (\bar{p}c)_{V-A}(\bar{u}p)_{V-A}, & O_2^p &= (\bar{p}_\alpha c_\beta)_{V-A}(\bar{u}_\beta p_\alpha)_{V-A}, \\
O_{3(5)} &= (\bar{u}c)_{V-A} \sum_q (\bar{q}q)_{V\mp A}, \\
O_{4(6)} &= (\bar{u}_\alpha c_\beta)_{V-A} \sum_q (\bar{q}_\beta q_\alpha)_{V\mp A}, \\
O_{8g} &= -\frac{g_s}{8\pi^2} m_c \bar{u} \sigma_{\mu\nu} (1 + \gamma_5) G^{\mu\nu} c,
\end{aligned} \tag{18}$$

with O_3 – O_6 being the QCD penguin operators and $(\bar{q}_1 q_2)_{V\mp A} \equiv \bar{q}_1 \gamma_\mu (1 \pm \gamma_5) q_2$. We shall work in the QCD factorization (QCDF) approach [54,55] to evaluate the hadronic matrix elements, but keep in mind that we employ this approach simply for a crude estimate of the penguin amplitudes because the charm quark mass is not heavy enough and $1/m_c$ power corrections are so large that a sensible heavy quark expansion is not allowed.

Let us first consider the penguin amplitudes in $D \rightarrow P_1 P_2$ decays:

$$\begin{aligned}
P_{P_1 P_2}^p &= \frac{G_F}{\sqrt{2}} [a_4^p(P_1 P_2) + r_\chi^p a_6^p(P_1 P_2)] f_{P_2} (m_D^2 - m_{P_1}^2) \\
&\quad \times F_0^{DP_1}(m_{P_2}^2), \\
PE_{P_1 P_2}^p &= \frac{G_F}{\sqrt{2}} (f_D f_{P_1} f_{P_2}) [b_3^p]_{P_1 P_2}, \\
PA_{P_1 P_2}^p &= \frac{G_F}{\sqrt{2}} (f_D f_{P_1} f_{P_2}) [b_4^p]_{P_1 P_2},
\end{aligned} \tag{19}$$

where $p = d, s$ and

$$r_\chi^p(\mu) = \frac{2m_p^2}{m_c(\mu)(m_2 + m_1)(\mu)} \tag{20}$$

is a chiral factor. Here we have followed the conventional Bauer-Stech-Wirbel definition for the form factor F_0^{DP} [56]. The explicit expressions of the flavor operators a_4^p and a_6^p will be given in Eq. (41) below. The annihilation operators $b_{3,4}^p$ are given by

$$\begin{aligned}
b_3^p &= \frac{C_F}{N_c^2} [c_3 A_1^i + c_5 (A_3^i + A_3^f) + N_c c_6 A_3^f], \\
b_4^p &= \frac{C_F}{N_c^2} [c_4 A_1^i + c_6 A_2^i],
\end{aligned} \tag{21}$$

where the annihilation amplitudes $A_{1,2,3}^{i,f}$ are defined in Ref. [55].

In practical calculations of QCDF, the superscript ‘‘ p ’’ can be omitted for a_3, a_5, b_3 and b_4 . Hence, we have $PE^s = PE^d$, for instance. For a_4^p and a_6^p , the terms dictating the p dependence are $G_{M_2}(s_p)$ and $\hat{G}_{M_2}(s_p)$, respectively, defined in Eq. (43) below.

III. DIRECT CP VIOLATION IN $D \rightarrow PP$ DECAYS

In Ref. [37], we have discussed direct CP violation in $D \rightarrow PP$ decays. Here we will update and improve the results. For example, we will discuss the issue of end-point divergences with the penguin-exchange and penguin-annihilation amplitudes. We will also consider the uncertainties connected with long-distance contribution to the penguin-exchange amplitude. We shall keep some necessary formula presented in [37] for ensuing discussions.

A. Tree-level CP violation

Direct CP asymmetry in hadronic charm decays defined by

$$a_{CP}^{\text{dir}}(f) = \frac{\Gamma(D \rightarrow f) - \Gamma(\bar{D} \rightarrow \bar{f})}{\Gamma(D \rightarrow f) + \Gamma(\bar{D} \rightarrow \bar{f})} \tag{22}$$

can occur even at the tree level [57]. As stressed in [36,37], the estimate of the tree-level CP violation $a_{\text{dir}}^{\text{(tree)}}$ should be trustworthy since the magnitude and the relative strong phase of each individual topological tree amplitude in

TABLE III. Direct CP asymmetries (in units of 10^{-3}) of $D \rightarrow PP$ decays, where $a_{\text{dir}}^{(\text{tree})}$ denotes CP asymmetry arising from purely tree amplitudes. The superscript (t + p) denotes tree plus QCD-penguin amplitudes, (t + pa) for tree plus weak penguin-annihilation (PE and PA) amplitudes and “tot” for the total amplitude. The first (second) entry in $D^0 \rightarrow \eta\eta, \eta\eta', K^+K^-$ and $K_S K_S$ is for Solution I (II) of E_d and E_s [Eq. (16)]. For QCD-penguin exchange PE , we assume that it is similar to the topological E amplitude [see Eq. (33)]. For comparison, The predicted results of $a_{\text{dir}}^{(\text{tot})}$ in [53] for both the negative (former) and positive (latter) solutions for the phase δ_i are also presented.

Decay mode	$a_{\text{dir}}^{(\text{tree})}$	$a_{\text{dir}}^{(\text{t+p})}$	$a_{\text{dir}}^{(\text{t+pa})}$	$a_{\text{dir}}^{(\text{tot})}$ (this work)	$a_{\text{dir}}^{(\text{tot})}$ [53]
$D^0 \rightarrow \pi^+\pi^-$	0	0.03 ± 0.01	0.78 ± 0.22	0.80 ± 0.22	$1.17 \pm 0.20/1.18 \pm 0.20$
$D^0 \rightarrow \pi^0\pi^0$	0	0.27 ± 0.01	0.55 ± 0.30	0.82 ± 0.30	$0.04 \pm 0.09/0.79 \pm 0.10$
$D^0 \rightarrow \pi^0\eta$	0.78 ± 0.01	0.48 ± 0.01	0.24 ± 0.28	-0.05 ± 0.28	
$D^0 \rightarrow \pi^0\eta'$	-0.43 ± 0.01	-0.56 ± 0.01	-0.01 ± 0.17	-0.15 ± 0.17	
$D^0 \rightarrow \eta\eta$	-0.28 ± 0.01	-0.28 ± 0.01	-0.51 ± 0.07	-0.52 ± 0.07	
	-0.37 ± 0.01	-0.44 ± 0.01	-0.58 ± 0.07	-0.65 ± 0.07	
$D^0 \rightarrow \eta\eta'$	0.51 ± 0.00	0.09 ± 0.00	0.72 ± 0.22	0.29 ± 0.21	
	0.46 ± 0.01	0.16 ± 0.00	0.52 ± 0.15	0.22 ± 0.15	
$D^0 \rightarrow K^+K^-$	0	0.08 ± 0.00	-0.41 ± 0.14	-0.33 ± 0.14	$-0.47 \pm 0.08/ -0.46 \pm 0.08$
	0	-0.01 ± 0.00	-0.43 ± 0.12	-0.44 ± 0.12	
$D^0 \rightarrow K_S K_S$	-1.05	-1.05	-1.05	-1.05	$0.43 \pm 0.07/0.38 \pm 0.07$
	-1.99	-1.99	-1.99	-1.99	
$D^+ \rightarrow \pi^+\pi^0$	0	0	0	0	
$D^+ \rightarrow \pi^+\eta$	0.37 ± 0.02	0.07 ± 0.01	-0.34 ± 0.22	-0.63 ± 0.23	
$D^+ \rightarrow \pi^+\eta'$	-0.26 ± 0.02	-0.45 ± 0.03	0.30 ± 0.18	0.11 ± 0.18	
$D^+ \rightarrow K^+K_S$	-0.07 ± 0.02	0.10 ± 0.02	-0.46 ± 0.18	-0.30 ± 0.18	$-0.40 \pm 0.07/ -0.26 \pm 0.05$
$D_s^+ \rightarrow \pi^+K_S$	0.09 ± 0.03	-0.08 ± 0.03	0.61 ± 0.24	0.42 ± 0.24	$-0.40 \pm 0.07/ -0.36 \pm 0.07$
$D_s^+ \rightarrow \pi^0K^+$	-0.04 ± 0.06	-0.02 ± 0.04	0.89 ± 0.27	0.91 ± 0.27	$0.48 \pm 0.06/ -0.03 \pm 0.04$
$D_s^+ \rightarrow K^+\eta$	-0.75 ± 0.01	-0.92 ± 0.02	-0.64 ± 0.08	-0.81 ± 0.08	
$D_s^+ \rightarrow K^+\eta'$	0.34 ± 0.02	0.63 ± 0.03	-0.22 ± 0.24	0.07 ± 0.25	

charm decays can be extracted from the data. The predicted tree-level CP asymmetries for SCS modes are shown in Table III. We see that larger CP asymmetries can be achieved in those decay modes with interference between T and C or C and E . For example, $a_{\text{dir}}^{(\text{tree})}$ is of order 0.78×10^{-3} for $D^0 \rightarrow \pi^0\eta$ and -0.75×10^{-3} for $D_s^+ \rightarrow K^+\eta$.

Direct CP violation in $D^0 \rightarrow K_S K_S$ is given by

$$a_{\text{dir}}^{(\text{tree})}(D^0 \rightarrow K_S K_S) = \frac{2\text{Im}(\lambda_d \lambda_s^*) \text{Im}(E_d^* E_s)}{|\lambda_d|^2 |E_d - E_s|^2} = 1.3 \times 10^{-3} \frac{|E_d E_s|}{|E_d - E_s|^2} \sin \delta_{ds}, \quad (23)$$

where δ_{ds} is the strong phase of E_s relative to E_d . From the two solutions of E_d and E_s given in Eq. (16), we find⁴

$$a_{\text{dir}}^{(\text{tree})}(D^0 \rightarrow K_S K_S) = \begin{cases} -1.05 \times 10^{-3} & \text{Solution I,} \\ -1.99 \times 10^{-3} & \text{Solution II.} \end{cases} \quad (24)$$

For comparison, various predictions available in the literature are discussed here. $a_{\text{dir}}^{(\text{tree})}(K_S K_S) = 1.11 \times 10^{-3}$ was predicted in [39]. It ranges in $(0.38-0.43) \times 10^{-3}$ according

⁴In our previous work [37], we obtained $a_{\text{dir}}^{(\text{tree})}(D^0 \rightarrow K_S K_S) = -0.7 \times 10^{-3}$ for Solution I and -1.7×10^{-3} for Solution II.

to [53] (see also the last column of Table III). Both predictions are of the opposite sign from ours. As explained in [37], the positive sign of $a_{\text{dir}}^{(\text{tree})}(K_S K_S)$ given in [39] can be traced back to the phase of the W -exchange amplitude. In our case, the W -exchange amplitude is always in the second quadrant, while it lies in the third quadrant in [39] due to a sign flip. As noticed in passing, all the strong phases extracted from a fit to branching fractions are equivalent to those with a simultaneous sign flip. This explains why the strong phases of C and E in [39] are simultaneously opposite to ours in sign, and the sign difference between this work and [39] for $a_{\text{dir}}^{(\text{tree})}(K_S K_S)$. A measurement of $a_{\text{dir}}^{(\text{tree})}(D^0 \rightarrow K_S K_S)$ will resolve the discrete phase ambiguity. If it is measured to be negative as predicted by us, then the W -exchange amplitude should be in the second quadrant.

In [23], the direct CP violation in $D^0 \rightarrow K_S K_S$ was connected to that of $D^0 \rightarrow K^+ K^-$ via the relation

$$\frac{a_{\text{CP}}^{\text{dir}}(D^0 \rightarrow K_S K_S)}{a_{\text{CP}}^{\text{dir}}(D^0 \rightarrow K^+ K^-)} \sim \sqrt{\frac{\mathcal{B}(D^0 \rightarrow K^+ K^-)}{2\mathcal{B}(D^0 \rightarrow K_S K_S)}}. \quad (25)$$

Taking $a_{\text{CP}}^{\text{dir}}(D^0 \rightarrow K^+ K^-)$ to be $(-0.48 \pm 0.09) \times 10^{-3}$ from Table III and the measured branching fractions, the obtained result $a_{\text{CP}}^{\text{dir}}(D^0 \rightarrow K_S K_S) \approx -1.8 \times 10^{-3}$ is in

agreement in magnitude and sign with ours. $a_{CP}^{\text{dir}}(D^0 \rightarrow K_S K_S)$ was estimated to be 0.6% in [21], while an upper bound $|a_{\text{dir}}(D^0 \rightarrow K_S K_S)| \leq 1.1\%$ was set in [58].

The current experimental measurements are

$$a_{CP}^{\text{dir}}(K_S K_S) = \begin{cases} (-2.9 \pm 5.2 \pm 2.2)\% & \text{LHCb [59],} \\ (4.3 \pm 3.4 \pm 1.0)\% & \text{LHCb [60],} \\ (-0.02 \pm 1.53 \pm 0.17)\% & \text{Belle [61].} \end{cases} \quad (26)$$

Since LHCb has measured ΔA_{CP} to the accuracy of 10^{-3} , it is conceivable that an observation of CP violation in the decay $D^0 \rightarrow K_S K_S$ will be feasible in the near future.

B. Penguin-induced CP violation

Direct CP violation does not occur at the tree level in $D^0 \rightarrow K^+ K^-$ and $D^0 \rightarrow \pi^+ \pi^-$. In these two decays, the CP asymmetry arises from the interference between tree and penguin amplitudes. From Eq. (10), we obtain

$$a_{CP}^{\text{dir}}(\pi^+ \pi^-) = \frac{4\text{Im}[(\lambda_d - \lambda_s)\lambda_b^*] \text{Im}[(T^* + E^* + \Delta P^*)(T + E + \Delta P + \Sigma P - \Delta P)]_{\pi\pi}}{|\lambda_d - \lambda_s|^2 |T + E + \Delta P|_{\pi\pi}^2} \\ \approx 1.30 \times 10^{-3} \left| \frac{P_s + PE_s + PA_s}{T + E + \Delta P} \right|_{\pi\pi} \sin \delta_{\pi\pi}, \quad (27)$$

where $\delta_{\pi\pi}$ is the strong phase of $(P_s + PE_s + PA_s)_{\pi\pi}$ relative to $(T + E + \Delta P)_{\pi\pi}$ and likewise for $a_{CP}^{\text{dir}}(K^+ K^-)$. Hence,

$$\Delta a_{CP}^{\text{dir}} = -1.30 \times 10^{-3} \left(\left| \frac{P_d + PE_d + PA_d}{T + E - \Delta P} \right|_{KK} \sin \delta_{KK} + \left| \frac{P_s + PE_s + PA_s}{T + E + \Delta P} \right|_{\pi\pi} \sin \delta_{\pi\pi} \right), \quad (28)$$

with δ_{KK} being the strong phase of $(P_d + PE_d + PA_d)_{KK}$ relative to $(T + E - \Delta P)_{KK}$.

Using the input parameters for the light-cone distribution amplitudes of light mesons, quark masses and decay constants from Refs. [62,63] and form factors from Refs. [48,64], we find to the leading order in Λ_{QCD}/m_b in QCDF that

$$\begin{aligned} \left(\frac{P_d}{T} \right)_{\pi\pi} &= 0.226 e^{-i150^\circ}, & \left(\frac{P_s}{T} \right)_{\pi\pi} &= 0.231 e^{-i152^\circ}, & \left(\frac{\Delta P}{T} \right)_{\pi\pi} &= 0.010 e^{-i35^\circ}, \\ \left(\frac{P_d}{T} \right)_{KK} &= 0.220 e^{-i150^\circ}, & \left(\frac{P_s}{T} \right)_{KK} &= 0.227 e^{-i152^\circ}, & \left(\frac{\Delta P}{T} \right)_{KK} &= 0.010 e^{-i35^\circ}. \end{aligned} \quad (29)$$

It is obvious that $\Delta P = P_d - P_s$ arising from the difference in the d - and s -loop penguin contractions [see Eq. (41)] is very small compared to the tree amplitude. It is straightforward to show

$$\left(\frac{P_s}{T + E + \Delta P} \right)_{\pi\pi} = 0.32 e^{i176^\circ}, \quad \left(\frac{P_d}{T + E - \Delta P} \right)_{KK} = \begin{cases} 0.23 e^{-i164^\circ} \\ 0.23 e^{i178^\circ} \end{cases}, \quad (30)$$

for Solutions I and II of W -exchange amplitudes E_d and E_s [see Eq. (16)]. It follows from Eq. (28) that $a_{CP}^{\text{dir}}(\pi^+ \pi^-) = 0.029 \times 10^{-3}$, and

$$a_{CP}^{\text{dir}}(K^+ K^-) = \begin{cases} 0.082 \times 10^{-3} \\ -0.010 \times 10^{-3} \end{cases}, \quad \Delta a_{CP}^{\text{dir}} \approx \begin{cases} 0.05 \times 10^{-3} & \text{Solution I,} \\ -0.02 \times 10^{-3} & \text{Solution II.} \end{cases} \quad (31)$$

Evidently, CP asymmetries in $D^0 \rightarrow \pi^+ \pi^-$, $K^+ K^-$ induced by QCD penguins are very small mainly due to the strong phases $\delta_{\pi\pi}$ and δ_{KK} being not far from 180° .

So far we have only discussed leading-order QCDF calculations except for the chiral enhanced penguin contributions, namely, the a_6 terms in Eq. (19). For QCD-penguin power corrections, we shall consider weak penguin annihilation, namely, QCD-penguin exchange

PE and QCD-penguin annihilation PA which are formally of order $1/m_c$. However, it is well known that the weak penguin annihilation amplitudes in QCDF derived from Eq. (19) involve troublesome end-point divergences [54,55]. Hence, subleading power corrections generally can be studied only in a phenomenological way. For example, the end-point divergence is parametrized as [54,55]

$$X_A \equiv \int_0^1 \frac{dx}{1-x} = \ln\left(\frac{m_D}{\Lambda_h}\right) (1 + \rho_A e^{i\phi_A}), \quad (32)$$

with Λ_h being a typical hadronic scale of order 500 MeV, and ρ_A, ϕ_A being unknown real parameters. In hadronic B decays, the values of ρ_A and ϕ_A can be obtained from a fit to $B \rightarrow PP, VP$ and VV decays [65]. However, this is not available in charmed meson decays since penguin effects manifest mainly in CP violation. Therefore, we will not evaluate PE and PA in this way in the charm sector. Nevertheless, if we borrow typical values of ρ_A and ϕ_A from the B system, we find weak penguin annihilation contributions smaller than QCD penguin; for instance, $(PE/T)_{\pi\pi} \sim 0.04$ and $(PA/T)_{\pi\pi} \sim -0.02$. Therefore, it is safe to neglect short-distance contributions to weak penguin annihilation amplitudes.

As pointed out in [36], long-distance contributions to SCS decays, for example, $D^0 \rightarrow \pi^+\pi^-$, can proceed through the weak decay $D^0 \rightarrow K^+K^-$ followed by a resonantlike final-state rescattering as depicted in Fig. 2 of [36]. It has the same topology as the QCD-penguin exchange topological graph PE . Since weak penguin annihilation and FSIs are both of order $1/m_c$ in the heavy quark limit, this means FSIs could play an essential role in charm decays. Hence, it is plausible to assume that PE is of the same order of magnitude as E . In [36], we took $(PE)^{\text{LD}} = 1.60e^{i115^\circ}$ (in units of 10^{-6} GeV). In this work we will assign by choice the same magnitude and phase as E with 20% and 30° uncertainties, respectively, so that

$$(PE)^{\text{LD}} \approx (1.48 \pm 0.30)e^{i(120.9 \pm 30.0)^\circ}. \quad (33)$$

For simplicity, we shall assume its flavor independence, that is, $(PE)_d^{\text{LD}} = (PE)_s^{\text{LD}}$.

Including the long-distance contribution to penguin exchange PE , we get

$$\begin{aligned} (T, E, P, PE, PA)_{\pi\pi} &= (2.73, 0.82e^{-i142^\circ}, 0.87e^{i134^\circ}, 0.81e^{i111^\circ}, 0.25e^{-i43^\circ}), \\ (T, E, P, PE, PA)_{KK} &= (3.65, 1.20e^{-i85^\circ}, 1.21e^{i135^\circ}, 0.87e^{i111^\circ}, 0.45e^{-i5^\circ}). \end{aligned} \quad (38)$$

As a result,

$$\left(\frac{P + PE + PA}{T + E}\right)_{\pi\pi} = 0.66e^{i134^\circ}, \quad \left(\frac{P + PE + PA}{T + E}\right)_{KK} = 0.45e^{i131^\circ}. \quad (39)$$

This leads to the aforementioned value of Δa_{CP} . For comparison, in our case we have

$$\begin{aligned} \left(\frac{P_s + PE_s^{\text{LD}}}{T + E + \Delta P}\right)_{\pi\pi} &= 0.77e^{i114^\circ}, \\ \left(\frac{P_d + PE_d^{\text{LD}}}{T + E - \Delta P}\right)_{KK} &= \begin{cases} 0.45e^{i137^\circ} \\ 0.45e^{i120^\circ} \end{cases}. \end{aligned} \quad (34)$$

As shown in Table III, we see that the predicted CP violation denoted by $a_{\text{dir}}^{(\text{tot})}$ or $a_{\text{dir}}^{(\text{tree})}$ is at most of order 10^{-3} in the SM. Specifically, we have⁵

$$a_{CP}^{\text{dir}}(\pi^+\pi^-) = (0.80 \pm 0.22) \times 10^{-3}, \quad (35)$$

$$a_{CP}^{\text{dir}}(K^+K^-) = \begin{cases} (-0.33 \pm 0.14) \times 10^{-3} & \text{Solution I,} \\ (-0.44 \pm 0.12) \times 10^{-3} & \text{Solution II.} \end{cases} \quad (36)$$

Theoretical uncertainties are dominated by that of $(PE)^{\text{LD}}$. Hence, the CP asymmetry difference between $D^0 \rightarrow K^+K^-$ and $D^0 \rightarrow \pi^+\pi^-$ is given by

$$\Delta a_{CP}^{\text{dir}} = \begin{cases} (-1.14 \pm 0.26) \times 10^{-3} & \text{Solution I,} \\ (-1.25 \pm 0.25) \times 10^{-3} & \text{Solution II.} \end{cases} \quad (37)$$

Although our new results of $\Delta a_{CP}^{\text{dir}}$ are slightly smaller than the previous ones in [37], they have more realistic estimates of uncertainties and are consistent with the LHCb's new measurement in Eq. (4) within 1σ . Here we note in passing that the CP asymmetry predictions are very sensitive to $(PE)^{\text{LD}}$. Had we chosen to use the value of $1.60 \times 10^{-6}e^{i121^\circ}$ GeV, as done in [36], $\Delta a_{CP}^{\text{dir}}$ would become $(-1.24 \pm 0.26) \times 10^{-3}$ for Solution I and $(-1.34 \pm 0.25) \times 10^{-3}$ for Solution II.

C. Comparison with Li *et al.* [39]

Based on the so-called factorization-assisted topological-amplitude approach, an estimate of $\Delta a_{CP} = -1.00 \times 10^{-3}$ in the SM was made in [39]. In this work, the topological amplitudes in units of 10^{-6} GeV are given by⁶

⁵Since Eqs. (34) and (27) lead to $a_{CP}^{\text{dir}}(\pi^+\pi^-) = 0.91 \times 10^{-3}$ and $a_{CP}^{\text{dir}}(K^+K^-) = -0.40 \times 10^{-3}$ for Solution I and -0.51×10^{-3} for Solution II, the reader may wonder why they are slightly larger in magnitude than the final results presented in Table III. Such a difference is related to the fact that the predictions are made, as alluded to in footnote 3, statistically and the fact that CP asymmetries are not linear in the parameters.

⁶In terms of the notation of [39], P, PE, PA correspond to P_C, P_E and P_A , respectively.

$$(T, E, P, PE)_{\pi\pi} = (3.00, 1.64e^{i136^\circ}, 0.69e^{-i152^\circ}, 1.48e^{i121^\circ}),$$

$$(T, E, P, PE)_{KK} = \begin{cases} (3.96, 0.93e^{i101^\circ}, 0.88e^{-i150^\circ}, 1.48e^{i121^\circ}) & \text{Solution I,} \\ (3.96, 2.10e^{i107^\circ}, 0.88e^{-i150^\circ}, 1.48e^{i121^\circ}) & \text{Solution II.} \end{cases} \quad (40)$$

There are three crucial differences between this work and [39]: (i) the phase of E amplitudes is in the second quadrant in the former while in the third or fourth quadrant in the latter, (ii) the phase of the penguin amplitude P is in the third quadrant in our work while in the second quadrant in [39], and (iii) our PE amplitude comes from long-distance final-state rescattering as we have neglected short-distance contributions to weak penguin annihilation amplitudes PE and PA . As discussed in passing, there is a discrete phase ambiguity for the phases of C , E and A topological amplitudes in our analysis. Presumably, a measurement

of $a_{CP}^{\text{dir}}(D^0 \rightarrow K_S K_S)$ will resolve the discrete phase ambiguity for the E amplitude. However, the phase of the penguin amplitude is calculated in theory. Let us examine this issue as follows.

Consider the penguin amplitude $P_{P_1 P_2}^p$ given in Eq. (19). Within the framework of QCDF, the flavor operators $a_{4,6}^p$ are basically the Wilson coefficients in conjunction with short-distance nonfactorizable corrections such as vertex corrections V_i , penguin contractions \mathcal{P}_i and hard spectator interactions H_i :

$$a_4^p(P_1 P_2) = \left(c_4 + \frac{c_3}{N_c} \right) + \frac{c_3}{N_c} \frac{C_F \alpha_s}{4\pi} \left[V_4(P_2) + \frac{4\pi^2}{N_c} H_4(P_1 P_2) \right] + \mathcal{P}_4^p(P_2),$$

$$a_6^p(P_1 P_2) = \left(c_6 + \frac{c_5}{N_c} \right) + \frac{c_5}{N_c} \frac{C_F \alpha_s}{4\pi} \left[V_6(P_2) + \frac{4\pi^2}{N_c} H_6(P_1 P_2) \right] + \mathcal{P}_6^p(P_2), \quad (41)$$

where the explicit expressions of V_i and H_i can be found in [55]. The order α_s corrections from penguin contraction read [55]

$$\mathcal{P}_4^p = \frac{C_F \alpha_s}{4\pi N_c} \left\{ c_1 \left[\frac{4}{3} \ln \frac{m_c}{\mu} + \frac{2}{3} - G_{M_2}(s_p) \right] + c_3 \left[\frac{8}{3} \ln \frac{m_c}{\mu} + \frac{4}{3} - G_{M_2}(s_u) - G_{M_2}(1) \right] \right. \\ \left. + (c_4 + c_6) \left[\frac{16}{3} \ln \frac{m_c}{\mu} - G_{M_2}(s_u) - G_{M_2}(s_d) - G_{M_2}(s_s) - G_{M_2}(1) \right] - 2c_{8g}^{\text{eff}} \int_0^1 \frac{dx}{1-x} \Phi_{M_2}(x) \right\},$$

$$\mathcal{P}_6^p = \frac{C_F \alpha_s}{4\pi N_c} \left\{ c_1 \left[\frac{4}{3} \ln \frac{m_c}{\mu} + \frac{2}{3} - \hat{G}_{M_2}(s_p) \right] + c_3 \left[\frac{8}{3} \ln \frac{m_c}{\mu} + \frac{4}{3} - \hat{G}_{M_2}(s_u) - \hat{G}_{M_2}(1) \right] \right. \\ \left. + (c_4 + c_6) \left[\frac{16}{3} \ln \frac{m_c}{\mu} - \hat{G}_{M_2}(s_u) - \hat{G}_{M_2}(s_d) - \hat{G}_{M_2}(s_s) - \hat{G}_{M_2}(1) \right] - 2c_{8g}^{\text{eff}} \right\}, \quad (42)$$

where $c_{8g}^{\text{eff}} = c_{8g} + c_5$, $s_i = m_i^2/m_c^2$,

$$G_{M_2}(s) = \int_0^1 dx G(s, 1-x) \Phi_{M_2}(x), \quad \hat{G}_{M_2}(s) = \int_0^1 dx G(s, 1-x) \hat{\Phi}_{M_2}(x), \quad (43)$$

and $G(s, x) = -4 \int_0^1 du u(1-u) \ln[s - u(1-u)x]$. Here Φ_{M_2} ($\hat{\Phi}_{M_2}$) is the twist-2 (-3) light-cone distribution amplitude for the meson M_2 .

In [39], the flavor operators $a_{4,6}$ and $a_{1,2}$ are taken to be

$$a_1(\mu) = c_1(\mu) + \frac{c_2(\mu)}{N_c}, \quad a_2(\mu) = c_2(\mu) + c_1(\mu) \left[\frac{1}{N_c} + \chi_{nf} e^{i\phi} \right],$$

$$a_{4,6}(\mu) = c_{4,6}(\mu) + c_{3,5}(\mu) \left[\frac{1}{N_c} + \chi_{nf} e^{i\phi} \right], \quad (44)$$

Comparing Eq. (44) with Eq. (41), we see that the source of the QCD penguin's strong phase is assumed to be the same as that of a_2 in [39], while it arises from nonfactorizable contributions in QCDF. In other words, while we consider the effects of vertex corrections, penguin contractions and hard spectator interactions for the QCD penguin amplitude, these effects are parametrized in [39] in terms of χ_{nf} and ϕ , which are determined from a global fit to the measured branching fractions. Since the color-suppressed C amplitude in [39] is in the second quadrant, so is the penguin amplitude. This explains the difference between our work and [39] for the QCD penguin amplitudes.

D. Comparison with Chala *et al.* [31]

Based on the light-cone sum rule calculations of

$$\begin{aligned} \left| \frac{P}{T+E} \right|_{\pi\pi} &= 0.093 \pm 0.011, \\ \left| \frac{P}{T+E} \right|_{KK} &= 0.075 \pm 0.015, \end{aligned} \quad (45)$$

Khodjamirian and Petrov [35] argued an upper bound in the SM, $|\Delta a_{CP}^{\text{SM}}| \leq (2.0 \pm 0.3) \times 10^{-4}$. Including higher-twist effects in the operator product expansion for the underlying correlation functions which are expected to be

$$\begin{aligned} \left| \frac{P}{T+E} \right|_{\pi\pi} &= 0.093 \pm 0.030, \\ \left| \frac{P}{T+E} \right|_{KK} &= 0.075 \pm 0.035, \end{aligned} \quad (46)$$

Chala *et al.* [31] claimed a modification of the SM bound, $|\Delta a_{CP}^{\text{SM}}| \leq (2.0 \pm 1.0) \times 10^{-4}$.

This conclusion seems to be very naive. First, as stated in [35], Khodjamirian and Petrov have neglected the contributions from the penguin operators $O_{i=3,\dots,6,8g}$ due to their small Wilson coefficients. This means they only considered the penguin contraction from the tree operators $O_{1,2}$. Consequently,

$$a_4^p = a_6^p \approx \frac{C_F \alpha_s}{4\pi N_c} c_1 \left[\frac{4}{3} \ln \frac{m_c}{\mu} + \frac{2}{3} - G_{M_2}(s_p) \right]. \quad (47)$$

Second, penguin-exchange and penguin-annihilation contributions have not been considered, not mentioning the possible final-state resattering effect on PE . They play an essential role in understanding the LHCb measurement of Δa_{CP} . Otherwise, it is premature to claim the necessity of new physics in this regard.

IV. $D \rightarrow VP$ DECAYS

In the treatment of $D \rightarrow VP$ decays, we continue to use the same topological diagram notation as in the PP decays,

except that a subscript of V or P is attached to the flavor amplitudes and the associated strong phases to denote whether the spectator quark in the charmed meson ends up in the vector or pseudoscalar meson in the final state. The V -type and P -type parameters are completely independent *a priori*, though certain relations can be established under the factorization assumption.

A. Topological amplitudes

The partial decay widths of the D meson into a vector and pseudoscalar mesons are usually expressed in two different ways:

$$\Gamma(D \rightarrow VP) = \frac{p_c^3}{8\pi m_D^2} |\tilde{\mathcal{M}}|^2, \quad (48)$$

and

$$\Gamma(D \rightarrow VP) = \frac{p_c^3}{8\pi m_V^2} |\mathcal{M}|^2. \quad (49)$$

Even though both formulas have the same cubic power dependence on p_c (as required for a P-wave configuration), a main difference resides in the fact that the latter has incorporated an additional SU(3)-breaking factor for the phase space, resulting from the sum of possible polarizations of the vector meson in the final state.

By performing a χ^2 fit to the CF $D \rightarrow VP$ decays, we extract the magnitudes and strong phases of the topological amplitudes T_V, C_V, E_V, A_V and T_P, C_P, E_P, A_P from the measured partial widths through Eq. (48) or (49) and find many possible solutions with local χ^2 minima. Here we take the convention that all strong phases are defined relative to the T_V amplitude. In 2016 we have performed a detailed analysis and obtained some best χ^2 fit solutions (A) and (S) through Eqs. (48) and (49), respectively [41]. It turns out that solutions (S) give a better description for SCS decays such as $D^0 \rightarrow \pi^+ \rho^-$, $\pi^0 \rho^0$ and $D^+ \rightarrow \pi^+ \rho^0$, possibly because the additional SU(3)-breaking factor in phase space has been taken care of, as mentioned above. Hence, we will confine ourselves to using Eq. (49) and thus solutions (S) in this work.

The six best χ^2 -fit solutions (S1)–(S6), with $\chi_{\min}^2 < 10$, are listed in Table IV, where we have chosen the convention such that the central values of strong phases fall between 0 and 360 degrees, while noting again that a simultaneous sign flip of all strong phases is equally viable. The flavor amplitudes of all these solutions respect the hierarchy pattern, $|T_P| > |T_V| \gtrsim |C_P| > |C_V| \gtrsim |E_P| > |E_V| \gtrsim |A_{P,V}|$. As stressed in [41], the decay $D_s^+ \rightarrow \rho^0 \pi^+$ plays an essential role in the determination of the annihilation amplitudes $A_{V,P}$. Its large error in the branching fraction reflects in the large uncertainties in the magnitudes and strong phases of $A_{V,P}$, which will be improved once we have a better measurement of $D_s^+ \rightarrow \rho^0 \pi^+$.

While the size of each topological amplitude is similar across all solutions, the strong phases vary among the

TABLE IV. Fit results using Eq. (49) and $\phi = 43.5^\circ$. The amplitude sizes are quoted in units of 10^{-6} and the strong phases in units of degrees.

	(S1)	(S2)	(S3)	(S4)	(S5)	(S6)
$ T_V $	$2.18^{+0.06}_{-0.07}$	$2.18^{+0.06}_{-0.07}$	2.17 ± 0.06	$2.19^{+0.06}_{-0.07}$	$2.18^{+0.06}_{-0.07}$	2.18 ± 0.06
$ T_P $	3.41 ± 0.06	3.36 ± 0.06	3.51 ± 0.06	3.48 ± 0.06	3.50 ± 0.06	3.39 ± 0.06
δ_{T_P}	69 ± 3	286 ± 3	40^{+3}_{-4}	307^{+4}_{-3}	79^{+3}_{-4}	12 ± 3
$ C_V $	1.76 ± 0.04	1.76 ± 0.04	1.74 ± 0.04	1.75 ± 0.04	1.74 ± 0.04	1.76 ± 0.04
δ_{C_V}	278 ± 3	76 ± 3	195^{+4}_{-3}	152^{+3}_{-4}	235^{+4}_{-3}	221 ± 3
$ C_P $	2.10 ± 0.03	2.07 ± 0.03	2.04 ± 0.03	2.14 ± 0.03	2.07 ± 0.03	2.07 ± 0.03
δ_{C_P}	201 ± 1	201 ± 1	201 ± 1	159 ± 1	159 ± 1	201 ± 1
$ E_V $	0.27 ± 0.04	0.26 ± 0.04	0.40 ± 0.06	0.33 ± 0.05	0.38 ± 0.05	0.26 ± 0.04
δ_{E_V}	260^{+50}_{-20}	69^{+46}_{-21}	245^{+8}_{-9}	113^{+14}_{-11}	282^{+8}_{-10}	224^{+22}_{-40}
$ E_P $	$1.66^{+0.05}_{-0.06}$	$1.66^{+0.05}_{-0.06}$	1.66 ± 0.05	$1.66^{+0.05}_{-0.06}$	1.66 ± 0.05	$1.66^{+0.05}_{-0.06}$
δ_{E_P}	108 ± 3	108 ± 3	107 ± 3	251 ± 3	252 ± 3	108 ± 3
$ A_V $	0.19 ± 0.02	0.20 ± 0.03	0.22 ± 0.03	0.25 ± 0.02	0.26 ± 0.02	0.24 ± 0.03
δ_{A_V}	17^{+9}_{-12}	349^{+10}_{-8}	73 ± 7	355^{+13}_{-12}	27^{+8}_{-9}	68 ± 8
$ A_P $	0.22 ± 0.03	0.22 ± 0.03	0.19 ± 0.03	0.15 ± 0.03	$0.14^{+0.03}_{-0.02}$	0.16 ± 0.03
δ_{A_P}	342^{+12}_{-9}	24^{+9}_{-11}	108^{+9}_{-11}	20^{+12}_{-27}	13^{+45}_{-17}	98^{+11}_{-17}
χ^2_{\min}	5.438	5.603	5.604	7.345	7.495	7.956
Fit quality	0.1424	0.1326	0.1096	0.062	0.058	0.047

solutions except for those of C_P and E_P . We find $(\delta_{C_P}, \delta_{E_P})$ to be either $(201^\circ, 108^\circ)$ or $(159^\circ, 252^\circ)$. A close inspection tells us that Solutions (S1) and (S4) are close to each other in the sense that the corresponding amplitudes are similar in size,

except for $|A_V|$ and $|A_P|$, and the corresponding strong phases add up to roughly 360° . So are Solutions (S2) and (S5).

Although solutions in set (S) generally fit the Cabibbo-favored modes well [see Table V for results

TABLE V. Flavor amplitude decompositions, experimental branching fractions, and predicted branching fractions for the Cabibbo-favored $D \rightarrow VP$ decays. Here $s_\phi \equiv \sin \phi$, $c_\phi \equiv \cos \phi$ and $\lambda_{sd} \equiv V_{cs}^* V_{ud}$. The columns of $\mathcal{B}_{\text{theory}}(S3)$ and $\mathcal{B}_{\text{theory}}(S6)$ are predictions based on Solutions (S3) and (S6) shown in Table IV, respectively. All branching fractions are quoted in units of %.

Meson	Mode	Representation	\mathcal{B}_{exp}	$\mathcal{B}_{\text{theory}}(S3)$	$\mathcal{B}_{\text{theory}}(S6)$
D^0	$K^{*-}\pi^+$	$\lambda_{sd}(T_V + E_P)$	5.34 ± 0.41	5.39 ± 0.40	5.35 ± 0.40
	$K^-\rho^+$	$\lambda_{sd}(T_P + E_V)$	11.3 ± 0.7	11.4 ± 0.6	11.7 ± 0.8
	$\bar{K}^{*0}\pi^0$	$\frac{1}{\sqrt{2}}\lambda_{sd}(C_P - E_P)$	3.74 ± 0.27	3.67 ± 0.21	3.69 ± 0.21
	$\bar{K}^0\rho^0$	$\frac{1}{\sqrt{2}}\lambda_{sd}(C_V - E_V)$	$1.26^{+0.12}_{-0.16}$	1.30 ± 0.12	1.35 ± 0.13
	$\bar{K}^{*0}\eta$	$\lambda_{sd}\left[\frac{1}{\sqrt{2}}(C_P + E_P)c_\phi - E_Vs_\phi\right]$	1.02 ± 0.30	0.92 ± 0.08	0.86 ± 0.12
	$\bar{K}^{*0}\eta'$	$-\lambda_{sd}\left[\frac{1}{\sqrt{2}}(C_P + E_P)s_\phi + E_Vc_\phi\right]$	<0.10	0.0048 ± 0.0004	0.0052 ± 0.0007
	$\bar{K}^0\omega$	$-\frac{1}{\sqrt{2}}\lambda_{sd}(C_V + E_V)$	2.22 ± 0.12	2.23 ± 0.16	2.17 ± 0.16
	$\bar{K}^0\phi$	$-\lambda_{sd}E_P$	0.830 ± 0.061	0.835 ± 0.054	0.838 ± 0.054
D^+	$\bar{K}^{*0}\pi^+$	$\lambda_{sd}(T_V + C_P)$	1.57 ± 0.13	1.59 ± 0.15	1.58 ± 0.15
	$\bar{K}^0\rho^+$	$\lambda_{sd}(T_P + C_V)$	$12.3^{+1.2}_{-0.7}$	12.5 ± 1.5	12.3 ± 1.5
D_s^+	$\bar{K}^{*0}K^+$	$\lambda_{sd}(C_P + A_V)$	3.92 ± 0.14	3.94 ± 0.18	3.94 ± 0.18
	\bar{K}^0K^{*+}	$\lambda_{sd}(C_V + A_P)$	5.4 ± 1.2	3.39 ± 0.21	3.10 ± 0.21
	$\rho^+\pi^0$	$\frac{1}{\sqrt{2}}\lambda_{sd}(A_P - A_V)$	\dots	0.024 ± 0.014	0.025 ± 0.016
	$\rho^+\eta$	$\lambda_{sd}\left[\frac{1}{\sqrt{2}}(A_P + A_V)c_\phi - T_Ps_\phi\right]$	8.9 ± 0.8	9.02 ± 0.37	8.86 ± 0.38
	$\rho^+\eta'$	$\lambda_{sd}\left[\frac{1}{\sqrt{2}}(A_P + A_V)s_\phi + T_Pc_\phi\right]$	5.8 ± 1.5	3.25 ± 0.12	2.92 ± 0.11
	$\pi^+\rho^0$	$\frac{1}{\sqrt{2}}\lambda_{sd}(A_V - A_P)$	0.020 ± 0.012	0.023 ± 0.014	0.024 ± 0.016
	$\pi^+\omega$	$\frac{1}{\sqrt{2}}\lambda_{sd}(A_V + A_P)$	0.19 ± 0.03^a	0.19 ± 0.04	0.19 ± 0.04
	$\pi^+\phi$	$\lambda_{sd}T_V$	4.5 ± 0.4	4.45 ± 0.24	4.49 ± 0.25

^aNew measurement from BESIII [67] has been taken into account in the world average.

TABLE VI. Same as Table V, but for the singly Cabibbo-suppressed decay modes. All branching fractions are quoted in units of 10^{-3} .

Mode	Representation	\mathcal{B}_{exp}	$\mathcal{B}_{\text{theo(S3)}}$	$\mathcal{B}_{\text{theo(S6)}}$
$D^0 \pi^+ \rho^-$	$\lambda_d(T_V + E_P) + \lambda_p(P_V^p + PA_P + PE_P)$	5.15 ± 0.25	4.72 ± 0.35	4.68 ± 0.35
$\pi^- \rho^+$	$\lambda_d(T_P + E_V) + \lambda_p(P_P^p + PA_V + PE_V)$	10.1 ± 0.4	8.81 ± 0.46	9.14 ± 0.60
$\pi^0 \rho^0$	$\frac{1}{2} \lambda_d(-C_P - C_V + E_P + E_V)$ $+ \lambda_p(P_P^p + P_V^p + PA_P + PA_V + PE_P + PE_V)$	3.86 ± 0.23	3.18 ± 0.19	3.92 ± 0.20
$K^+ K^{*-}$	$\lambda_s(T_V + E_P) + \lambda_p(P_V^p + PE_P + PA_P)$	1.65 ± 0.11	1.81 ± 0.14	1.79 ± 0.13
$K^- K^{*+}$	$\lambda_s(T_P + E_V) + \lambda_p(P_P^p + PE_V + PA_V)$	4.56 ± 0.21	3.35 ± 0.17	3.44 ± 0.23
$K^0 \bar{K}^{*0}$	$\lambda_d E_V + \lambda_s E_P + \lambda_p(PA_P + PA_V)$	0.246 ± 0.048	1.27 ± 0.10	1.04 ± 0.14
$\bar{K}^0 K^{*0}$	$\lambda_d E_P + \lambda_s E_V + \lambda_p(PA_P + PA_V)$	0.336 ± 0.063	1.27 ± 0.10	1.04 ± 0.14
$\pi^0 \omega$	$\frac{1}{2} \lambda_d(-C_V + C_P - E_P - E_V) + \lambda_p(P_P^p + P_V^p + PE_P + PE_V)$	0.117 ± 0.035	0.53 ± 0.09	0.22 ± 0.06
$\pi^0 \phi$	$\frac{1}{\sqrt{2}} \lambda_s C_P$	1.20 ± 0.04^a	0.64 ± 0.02	0.65 ± 0.02
$\eta \omega$	$\frac{1}{2} [\lambda_d(C_V + C_P + E_V + E_P) \cos \phi - \lambda_s C_V \sin \phi]$ $+ \lambda_p(P_P^p + P_V^p + PE_P + PE_V + PA_P + PA_V) \cos \phi$	1.98 ± 0.18	2.96 ± 0.13	2.56 ± 0.14
$\eta' \omega$	$\frac{1}{2} [\lambda_d(C_V + C_P + E_V + E_P) \sin \phi + \lambda_s C_V \cos \phi]$ $+ \lambda_p(P_P^p + P_V^p + PE_P + PE_V + PA_P + PA_V) \sin \phi$	\dots	0.03 ± 0.00	0.05 ± 0.01
$\eta \phi$	$\lambda_s [\frac{1}{\sqrt{2}} C_P \cos \phi - (E_V + E_P) \sin \phi] + \lambda_p(PA_P + PA_V) \sin \phi$	0.167 ± 0.034^a	0.24 ± 0.02	0.29 ± 0.03
$\eta \rho^0$	$\frac{1}{2} [\lambda_d(C_V - C_P - E_V - E_P) \cos \phi - \lambda_s \sqrt{2} C_V \sin \phi]$ $+ \lambda_p(P_P^p + P_V^p + PE_P + PE_V) \cos \phi$	\dots	0.31 ± 0.05	0.84 ± 0.10
$\eta' \rho^0$	$\frac{1}{2} [\lambda_d(C_V - C_P - E_V - E_P) \sin \phi + \lambda_s \sqrt{2} C_V \cos \phi]$ $+ \lambda_p(P_P^p + P_V^p + PE_P + PE_V) \sin \phi$	\dots	0.11 ± 0.01	0.10 ± 0.01
$D^+ \pi^+ \rho^0$	$\frac{1}{\sqrt{2}} [\lambda_d(T_V + C_P - A_P + A_V) + \lambda_p(P_V^p - P_P^p + PE_P - PE_V)]$	0.83 ± 0.15	0.70 ± 0.10	0.61 ± 0.10
$\pi^0 \rho^+$	$\frac{1}{\sqrt{2}} [\lambda_d(T_P + C_V + A_P - A_V) + \lambda_p(P_P^p - P_V^p + PE_V - PE_P)]$	\dots	4.43 ± 0.61	4.53 ± 0.64
$\pi^+ \omega$	$\frac{1}{\sqrt{2}} [\lambda_d(T_V + C_P + A_P + A_V) + \lambda_p(P_P^p + P_V^p + PE_P + PE_V)]$	0.28 ± 0.06	0.22 ± 0.06	0.26 ± 0.07
$\pi^+ \phi$	$\lambda_s C_P$	5.68 ± 0.11^a	3.27 ± 0.11	3.35 ± 0.11
$\eta \rho^+$	$\frac{1}{\sqrt{2}} [\lambda_d(T_P + C_V + A_V + A_P) \cos \phi - \lambda_s \sqrt{2} C_V \sin \phi]$ $+ \lambda_p(P_P^p + P_V^p + PE_P + PE_V) \cos \phi$	\dots	1.53 ± 0.49	1.02 ± 0.34
$\eta' \rho^+$	$\frac{1}{\sqrt{2}} [\lambda_d(T_P + C_V + A_V + A_P) \sin \phi + \lambda_s \sqrt{2} C_V \cos \phi]$ $+ \lambda_p(P_P^p + P_V^p + PE_P + PE_V) \sin \phi$	\dots	1.16 ± 0.11	1.03 ± 0.11
$K^+ \bar{K}^{*0}$	$\lambda_d A_V + \lambda_s T_V + \lambda_p(P_V^p + PE_P)$	$3.83_{-0.21}^{+0.14}$	3.87 ± 0.23	3.82 ± 0.25
$\bar{K}^0 K^{*+}$	$\lambda_d A_P + \lambda_s T_P + \lambda_p(P_P^p + PE_V)$	34 ± 16	10.20 ± 0.40	9.80 ± 0.41
$D_s^+ \pi^+ K^{*0}$	$\lambda_d T_V + \lambda_s A_V + \lambda_p(P_V^p + PE_P)$	2.13 ± 0.36	3.69 ± 0.23	3.65 ± 0.24
$\pi^0 K^{*+}$	$\frac{1}{\sqrt{2}} [\lambda_d C_V - \lambda_s A_V - \lambda_p(P_V^p + PE_P)]$	\dots	1.12 ± 0.07	1.02 ± 0.07
$K^+ \rho^0$	$\frac{1}{\sqrt{2}} [\lambda_d C_P - \lambda_s A_P - \lambda_p(P_P^p + PE_V)]$	2.5 ± 0.4	2.10 ± 0.10	2.10 ± 0.10
$K^0 \rho^+$	$\lambda_d T_P + \lambda_s A_P + \lambda_p(P_P^p + PE_V)$	\dots	11.80 ± 0.47	11.47 ± 0.48
ηK^{*+}	$\frac{1}{\sqrt{2}} \{ [\lambda_d C_V + \lambda_s A_V + \lambda_p(P_V^p + PE_P)] \cos \phi$ $- [\lambda_s (T_P + C_V + A_P) + \lambda_p(P_P^p + PE_V)] \sin \phi \}$	\dots	0.60 ± 0.21	0.64 ± 0.20
$\eta' K^{*+}$	$\frac{1}{\sqrt{2}} \{ [\lambda_d C_V + \lambda_s A_V + \lambda_p(P_V^p + PE_P)] \sin \phi$ $- [\lambda_s (T_P + C_V + A_P) + \lambda_p(P_P^p + PE_V)] \cos \phi \}$	\dots	0.38 ± 0.02	0.33 ± 0.02
$K^+ \omega$	$\frac{1}{\sqrt{2}} [\lambda_d C_P + \lambda_s A_P + \lambda_p(P_P^p + PE_V)]$	0.87 ± 0.25^b	2.02 ± 0.09	2.12 ± 0.10
$K^+ \phi$	$\lambda_s (T_V + C_P + A_V) + \lambda_p(P_V^p + PE_P)$	0.182 ± 0.041	0.13 ± 0.02	0.12 ± 0.02

^aNew measurements from BESIII [68] have been taken into account in the world average.^bData from BESIII [67].

based on Solutions (S3) and (S6)], there are two exceptions, namely, $D_s^+ \rightarrow \bar{K}^0 K^{*+}$ and $\rho^+ \eta'$, where the predictions are smaller than the experimental results. The first mode was measured three decades ago with a

relatively large uncertainty [66], and the experimental result was likely to be overestimated. The second mode has a decay amplitude respecting a sum rule [41]:

$$\begin{aligned} \mathcal{M}(D_s^+ \rightarrow \pi^+\omega) &= \cos\phi\mathcal{M}(D_s^+ \rightarrow \rho^+\eta) \\ &+ \sin\phi\mathcal{M}(D_s^+ \rightarrow \rho^+\eta'). \end{aligned} \quad (50)$$

Assuming this relation, the current data of $\mathcal{B}(D_s^+ \rightarrow \pi^+\omega)$ and $\mathcal{B}(D_s^+ \rightarrow \rho^+\eta)$ give the bounds $1.6\% < \mathcal{B}(D_s^+ \rightarrow \rho^+\eta') < 3.9\%$ at 1σ level, significantly lower than the current central value. A better determination of these branching fractions will be very helpful in settling the issues.

Various (S) solutions lead to very different predictions for some of the SCS decays. Especially, the $D^0 \rightarrow \pi^0\omega$ and $D^+ \rightarrow \pi^+\omega$ decays are very useful in discriminating among different solutions. We first consider the $\pi^0\rho^0$, $\pi^0\omega$ and $\eta\omega$ modes. Their topological amplitudes are given by

$$\begin{aligned} \mathcal{M}(D^0 \rightarrow \pi^0\omega) &= \frac{1}{2}\lambda_d(C_V - C_P + E_P + E_V), \\ \mathcal{M}(D^0 \rightarrow \pi^0\rho^0) &= \frac{1}{2}\lambda_d(C_V + C_P - E_P - E_V), \\ \mathcal{M}(D^0 \rightarrow \eta\omega) &= \frac{1}{2}\lambda_d(C_V + C_P + E_P + E_V)\cos\phi \\ &\quad - \frac{1}{\sqrt{2}}\lambda_s C_V \sin\phi. \end{aligned} \quad (51)$$

Since the magnitude of C_V is comparable to that of C_P , the smallness of $\mathcal{B}(D^0 \rightarrow \pi^0\omega)$, the sizable $\mathcal{B}(D^0 \rightarrow \eta\omega)$ and the large $\mathcal{B}(D^0 \rightarrow \pi^0\rho^0)$ imply that the strong phases of C_V and C_P should be close to each other. An inspection of Table IV indicates that the phase difference between C_V and C_P is large for Solutions (S1), (S2) and (S5). It turns out that (S2) and (S5) are definitely ruled out as they predict too large $\mathcal{B}(D^0 \rightarrow \pi^0\omega)$, with the central values of 4.65 and 3.91 (in units of 10^{-3}), respectively, while the measured value is 0.117 ± 0.035 (see Table VI). Solution (S1) gives a relatively better prediction of $\mathcal{B}(D^0 \rightarrow \pi^0\omega) = 0.62 \pm 0.13$ among the three solutions.

We next turn to the $\pi^+\rho^0$ and $\pi^+\omega$ modes. Neglecting the penguin contributions, their topological amplitudes read (see Table VI)

$$\begin{aligned} \mathcal{M}(D^+ \rightarrow \pi^+\rho^0) &= \frac{1}{\sqrt{2}}\lambda_d(T_V + C_P - A_P + A_V), \\ \mathcal{M}(D^+ \rightarrow \pi^+\omega) &= \frac{1}{\sqrt{2}}\lambda_d(T_V + C_P + A_P + A_V). \end{aligned} \quad (52)$$

It is well known that the CF decays $D_s^+ \rightarrow \pi^+\rho^0$ and $\pi^+\omega$ can only proceed through the W -annihilation topology

$$\begin{aligned} \mathcal{M}(D_s^+ \rightarrow \pi^+\rho^0) &= \frac{1}{\sqrt{2}}V_{cs}^*V_{ud}(A_V - A_P), \\ \mathcal{M}(D_s^+ \rightarrow \pi^+\omega) &= \frac{1}{\sqrt{2}}V_{cs}^*V_{ud}(A_V + A_P). \end{aligned} \quad (53)$$

The extremely small branching fraction of $D_s^+ \rightarrow \pi^+\rho^0$ compared to $D_s^+ \rightarrow \pi^+\omega$ (see Table V) implies that A_V and

A_P should be comparable in magnitude and roughly parallel to each other with a phase difference not more than 30° . At a first glance, it is tempting to argue from Eq. (52) that $D^+ \rightarrow \pi^+\omega$ should have a rate larger than $D^+ \rightarrow \pi^+\rho^0$. Experimentally, it is the other way around [46]:

$$\begin{aligned} \mathcal{B}(D^+ \rightarrow \pi^+\rho^0) &= (0.83 \pm 0.15) \times 10^{-3}, \\ \mathcal{B}(D^+ \rightarrow \pi^+\omega) &= (0.28 \pm 0.06) \times 10^{-3}. \end{aligned} \quad (54)$$

Since C_P is comparable to T_V in magnitude, there is a large cancellation between T_V and C_P . As a consequence, the rates of $\pi^+\rho^0$ and $\pi^+\omega$ become sensitive to the strong phases of the small annihilation amplitudes A_V and A_P . It turns out that A_V should be in the fourth quadrant while A_P in the third quadrant in order to satisfy the experimental constraints from Eq. (54). We find only Solutions (S3) and (S6) in line with this requirement (see Table IV) and yielding predictions in agreement with experiment for $\pi^+\rho^0$ and $\pi^+\omega$ (see Table VI). For Solutions (S1), (S2), (S4) and (S5), the branching fractions of $D^+ \rightarrow \pi^+\rho^0$ and $D^+ \rightarrow \pi^+\omega$ (in units of 10^{-3}) are found to have the central values (0.45, 1.06), (0.87, 0.98), (0.67, 1.05), (0.96, 1.76), respectively. All these solutions imply that the latter is larger than the former in rates, in contradiction with experiment.

Finally, we comment on two of the D_s^+ decay modes: $K^+\rho^0$ and $K^+\omega$. From Table VI, we see that

$$\begin{aligned} \mathcal{M}(D_s^+ \rightarrow K^+\rho^0) &= \frac{1}{\sqrt{2}}(\lambda_d C_P - \lambda_s A_P), \\ \mathcal{M}(D_s^+ \rightarrow K^+\omega) &= \frac{1}{\sqrt{2}}(\lambda_d C_P + \lambda_s A_P). \end{aligned} \quad (55)$$

Since $|C_P| \gg |A_P|$, it is expected that the two modes have similar branching fractions of order 2×10^{-3} . However, the recent BESIII experiment yields $\mathcal{B}(D_s^+ \rightarrow K^+\omega) = (0.87 \pm 0.25) \times 10^{-3}$ [67]. The $\rho - \omega$ mixing effect to be mentioned below in Eq. (63) in principle can push up (down) the rate of $K^+\rho^0$ ($K^+\omega$). For the mixing angle $\epsilon = -0.12$ [see Eq. (63) and note a sign difference from [69]], we find $\mathcal{B}(D_s^+ \rightarrow K^+\rho^0) = (2.63 \pm 0.11) \times 10^{-3}$ and $\mathcal{B}(D_s^+ \rightarrow K^+\omega) = (1.65 \pm 0.09) \times 10^{-3}$. The former is now in better agreement with experiment, but the latter is still too large compared to the data. The $\omega - \phi$ mixing also does not help much. Moreover, in our framework we do not need $\rho - \omega$ mixing to explain the smallness of $D^0 \rightarrow \pi^0\omega$ and $D^+ \rightarrow \pi^+\omega$. Therefore, the issue with $D_s^+ \rightarrow K^+\omega$ remains to be resolved.

B. Flavor SU(3) symmetry breaking

As noted in passing, a most noticeable example of SU(3) breaking in the PP sector lies in the decays $D^0 \rightarrow K^+K^-$

and $D^0 \rightarrow \pi^+ \pi^-$. Experimentally, the rate of the former is larger than that of the latter by a factor of 2.8. More precisely, $|T + E|_{KK}/|T + E|_{\pi\pi} \approx 1.80$, implying a large SU(3) breaking effect in the amplitude of $T + E$. However, it is the other way around for the counterparts in the VP sector where we have $\Gamma(K^+ K^{*-}) < \Gamma(\pi^+ \rho^-)$ and $\Gamma(K^- K^{*+}) < \Gamma(\pi^- \rho^+)$. Since the available phase space is proportional to p_c^3/m_V^2 in the convention of Eq. (49), this explains why $\Gamma(D^0 \rightarrow KK^*) < \Gamma(D^0 \rightarrow \pi\rho)$ owing to the fact that $p_c(\pi\rho) = 764$ MeV and $p_c(KK^*) = 608$ MeV. From the measured branching fractions, we find by ignoring the penguin amplitudes that

$$\frac{|T_V + E_P|_{\pi^+\rho^-}}{|T_V + E_P|_{K^+K^{*-}}} = 1.08, \quad \frac{|T_P + E_V|_{\pi^-\rho^+}}{|T_V + E_P|_{K^-K^{*+}}} = 0.91. \quad (56)$$

This implies that SU(3) breaking in the amplitudes of $T_V + E_P$ and $T_P + E_V$ is small, contrary to the PP case.

In Table VI, we show the calculated branching fractions of SCS $D \rightarrow VP$ decays using Solutions (S3) and (S6). It is clear that Solution (S6) is slightly better, though the predicted $K^0 \bar{K}^{*0}$ and $\bar{K}^0 K^{*0}$ branching fractions are too large compared to the data in both solutions. SU(3) breaking effects in the color-allowed and color-suppressed amplitudes can be estimated provided they are factorizable:

$$\begin{aligned} T_V &= \frac{G_F}{\sqrt{2}} a_1(\bar{K}^* \pi) 2f_\pi m_{K^*} A_0^{DK^*}(m_\pi^2), \\ C_P &= \frac{G_F}{\sqrt{2}} a_2(\bar{K}^* \pi) 2f_{K^*} m_{K^*} F_1^{D\pi}(m_{K^*}^2), \\ T_P &= \frac{G_F}{\sqrt{2}} a_1(\bar{K}\rho) 2f_\rho m_\rho F_1^{DK}(m_\rho^2), \\ C_V &= \frac{G_F}{\sqrt{2}} a_2(\bar{K}\rho) 2f_K m_\rho A_0^{D\rho}(m_K^2). \end{aligned} \quad (57)$$

$$\begin{aligned} \mathcal{M}(D^0 \rightarrow \pi^+ \rho^-) &= \lambda_d(T_V + E_P^d), \\ \mathcal{M}(D^0 \rightarrow K^+ K^{*-}) &= \lambda_s(T_V + E_P^s), \\ \mathcal{M}(D^0 \rightarrow K^0 \bar{K}^{*0}) &= \lambda_s E_P^s + \lambda_d E_V^d, \end{aligned}$$

and

$$\begin{aligned} \mathcal{M}(D^0 \rightarrow \pi^0 \rho^0) &= \frac{1}{2} \lambda_d(C_P + C_V - E_P^d - E_V^d), \\ \mathcal{M}(D^0 \rightarrow \pi^0 \omega) &= \frac{1}{2} \lambda_d(C_V - C_P + E_P^d + E_V^d), \end{aligned} \quad (59)$$

with

$$\begin{aligned} E_V^d &= e_V^d e^{i\delta_V^d} E_V, & E_V^s &= e_V^s e^{i\delta_V^s} E_V, \\ E_P^d &= e_P^d e^{i\delta_P^d} E_P, & E_P^s &= e_P^s e^{i\delta_P^s} E_P, \end{aligned} \quad (60)$$

Hence,

$$\begin{aligned} \frac{T_V^{\pi\rho}}{T_V} &= \frac{a_1(\rho\pi) m_\rho A_0^{D\rho}(m_\pi^2)}{a_1(\bar{K}^* \pi) m_{K^*} A_0^{DK^*}(m_\pi^2)}, \\ \frac{T_P^{\pi\rho}}{T_P} &= \frac{a_1(\rho\pi) F_1^{D\pi}(m_\rho^2)}{a_1(\bar{K}\rho) F_1^{DK}(m_\rho^2)}. \end{aligned} \quad (58)$$

Assuming that $a_1(\rho\pi)$ is similar to $a_1(\bar{K}^* \pi)$ and $a_1(\bar{K}\rho)$, we find $T_V(\pi^+ \rho^-) \simeq 0.82T_V$, $T_P(\pi^- \rho^+) \simeq 0.92T_P$, $T_V(K^+ K^{*-}) \simeq 1.29T_V$ and $T_P(K^- K^{*+}) \simeq 1.28T_P$. Similar relations can be derived for the C_V and C_P amplitudes as well. These lead to two difficulties: (i) The sizable SU(3) breaking in the ratios $|T_V|_{\pi^+\rho^-}/|T_V|_{K^+K^{*-}} \simeq 0.64$ and $|T_P|_{\pi^-\rho^+}/|T_V|_{K^-K^{*+}} \simeq 0.72$ are not consistent with Eq. (56), and (ii) the branching fractions of $D^0 \rightarrow \pi^+ \rho^-$ and $D^0 \rightarrow \pi^- \rho^+$ will become smaller, while $\mathcal{B}(D^0 \rightarrow K^+ K^{*-})$ and $\mathcal{B}(D^0 \rightarrow K^- K^{*+})$ become larger. Hence, the discrepancy becomes even worse. In other words, the consideration of SU(3) breaking in the tree amplitudes $T_{V,P}$ and $C_{V,P}$ alone will render even larger deviations from the data in both Solutions (S3) and (S6).

A way out is to consider SU(3) breaking in the W -exchange amplitudes. Indeed, the too large rates predicted for $K^0 \bar{K}^{*0}$ and $\bar{K}^0 K^{*0}$ modes call for SU(3) breaking in the W -exchange amplitudes as both modes proceed through E_P and E_V . In the PP sector, we need SU(3) breaking in W -exchange in order to induce $D^0 \rightarrow K_S K_S$. Here we need SU(3) breaking again for a different reason, otherwise, the calculated $D^0 \rightarrow K^0 \bar{K}^{*0}$ and $\bar{K}^0 K^{*0}$ will be too large in rates. Since $|E_P| \gg |E_V|$, it is natural to expect that $|E_P|$ ($|E_V|$) has to be reduced (increased) after SU(3) breaking in order to accommodate the data. Writing

$$\begin{aligned} \mathcal{M}(D^0 \rightarrow \pi^- \rho^+) &= \lambda_d(T_P + E_V^d), \\ \mathcal{M}(D^0 \rightarrow K^- K^{*+}) &= \lambda_s(T_P + E_V^s), \\ \mathcal{M}(D^0 \rightarrow \bar{K}^0 K^{*0}) &= \lambda_s E_V^s + \lambda_d E_P^d, \end{aligned}$$

we are able to determine the eight unknown parameters $e_V^d, e_P^d, e_V^s, e_P^s$ and $\delta e_V^d, \delta e_P^d, \delta e_V^s, \delta e_P^s$ from the branching fractions of these eight modes. In the SU(3) limit, $e_{V,P}^{d,s} = 1$ and $\delta e_{V,P}^{d,s} = 0$. Note that among all the best-fit solutions (S), only (S3) and (S6) give exact solutions for the parameters $e_{V,P}^{d,s}$ and the phases $\delta e_{V,P}^{d,s}$ (i.e., $\chi^2 = 0$ in a fit to the eight SCS modes). There are six solutions for Solution (S6), listed in Table VII. All these schemes are equally good in explaining the first eight SCS modes in Table VI, whereas Scheme (iv) yields smallest SU(3) symmetry violation in $e_{V,P}^{d,s}$; namely, the deviations of them from unity are less than 50%.

TABLE VII. Solutions of the parameters $e_{V,P}^{d,s}$ and the phases $\delta e_{V,P}^{d,s}$ describing SU(3) breaking effects in the W -exchange amplitudes for Solution (S6).

	e_V^d	δe_V^d	e_P^d	δe_P^d	e_V^s	δe_V^s	e_P^s	δe_P^s
(i)	1.50	241	0.18	290	3.44	69	0.29	159
(ii)	1.50	241	0.18	290	3.44	69	0.76	358
(iii)	1.12	55	0.51	336	6.67	243	6.35	347
(iv)	1.12	55	0.51	336	1.30	111	0.68	149
(v)	2.09	53	1.03	356	2.90	222	0.19	341
(vi)	2.09	53	1.03	356	2.90	222	0.81	146

Branching fractions of SCS $D \rightarrow VP$ decays are predicted in Table VIII using the topological amplitudes given in Solution (S6). For SU(3) breaking effects in W -exchange amplitudes E_V and E_P , we specifically choose solution (iv) for SU(3) breaking parameters given in Table VII, though the results are very similar in other schemes. The decays $D^0 \rightarrow \pi^0 \phi$ and $D^+ \rightarrow \pi^+ \phi$ are special as they proceed only through the internal W -emission diagram C_P . Its SU(3) breaking can be estimated from Eq. (58) to be

$$\frac{C_P^{\pi\phi}}{C_P} = \frac{f_\phi}{f_{K^*}} \frac{m_\phi}{m_{K^*}} \frac{F_1^{D\pi}(m_\phi^2)}{F_1^{D\pi}(m_{K^*}^2)}. \quad (61)$$

For the q^2 dependence of the form factor we use

$$F_1^{D\pi}(q^2) = \frac{F_1^{D\pi}(0)}{[1 - (q^2/m_{D^*}^2)][1 - \alpha_1^{D\pi}(q^2/m_{D^*}^2)]}, \quad (62)$$

with $F_1^{D\pi}(0) = F_0^{D\pi}(0) = 0.666$ and $\alpha_1^{D\pi} = 0.24$, and find $C_P^{\pi\phi} = 1.37C_P$. The resulting $\mathcal{B}(D^0 \rightarrow \pi^0 \phi) = (1.22 \pm 0.04) \times 10^{-3}$ and $\mathcal{B}(D^+ \rightarrow \pi^+ \phi) = (6.29 \pm 0.21) \times 10^{-3}$ are consistent with experiment, though the latter is slightly large in the central value.

Comparison with the work of Qin et al. [69].—In Table VIII, we have compared our results of SCS $D \rightarrow VP$ branching fractions with that in the factorization-assisted topological approach [69] without and with the $\rho - \omega$ mixing, denoted by FAT and FAT[mix], respectively. The predicted $\mathcal{B}(D^0 \rightarrow \pi^0 \omega) = 0.85$ (in units of 10^{-3}) in FAT is far too large compared to the data of 0.117 ± 0.035 . In order to resolve this discrepancy, Qin et al. considered the $\rho - \omega$ mixing defined by

$$|\rho^0\rangle = |\rho_I^0\rangle - \epsilon|\omega_I\rangle, \quad |\omega\rangle = \epsilon|\rho_I^0\rangle + |\omega_I\rangle, \quad (63)$$

where $|\rho_I^0\rangle$ and $|\omega_I\rangle$ denote the isospin eigenstates. Using the mixing angle $\epsilon = 0.12$, the predicted branching fraction of $D^0 \rightarrow \pi^0 \omega$ is reduced to 0.18, while $\mathcal{B}(D^0 \rightarrow \pi^0 \rho^0)$ is increased from 3.55 to 3.83. However, the calculated $\mathcal{B}(D^+ \rightarrow \pi^+ \omega) = 0.80$ after taking into account of $\rho - \omega$ mixing is still too large compared to the experimental value of 0.28 ± 0.06 . As for the $D_s^+ \rightarrow K^+ \omega$ mode, it appears

TABLE VIII. Branching fractions (in units of 10^{-3}) of $D \rightarrow VP$ decays. The predictions made in the (S6) scheme have taken into account SU(3) breaking effects under solution (iv) (see Table VII). For QCD-penguin exchanges PE_V and PE_P , we assume that they are similar to the topological E_V and E_P amplitude, respectively [see Eq. (64)]. The results from [69] in the factorization-assisted topological approach without and with the $\rho - \omega$ mixing (denoted by FAT and FAT[mix], respectively) are listed for comparison.

	Mode	\mathcal{B} (This work)	\mathcal{B} (FAT)	\mathcal{B} (FAT[mix])	\mathcal{B}_{exp}	
D^0	$\pi^+ \rho^-$	5.12 ± 0.29	4.74	4.66	5.15 ± 0.25	
	$\pi^- \rho^+$	10.21 ± 0.91	10.2	10.0	10.1 ± 0.4	
	$\pi^0 \rho^0$	3.90 ± 0.26	3.55	3.83	3.86 ± 0.23	
	$K^+ K^{*-}$	1.68 ± 0.11	1.72	1.73	1.65 ± 0.11	
	$K^- K^{*+}$	4.43 ± 0.31	4.37	4.37	4.56 ± 0.21	
	$K^0 \bar{K}^{*0}$	0.27 ± 0.06	1.1	1.1	0.246 ± 0.048	
	$\bar{K}^0 K^{*0}$	0.32 ± 0.09	1.1	1.1	0.336 ± 0.063	
	$\pi^0 \omega$	0.12 ± 0.05	0.85	0.18	0.117 ± 0.035	
	$\pi^0 \phi$	1.22 ± 0.04	1.11	1.11	1.20 ± 0.04	
	$\eta \omega$	2.25 ± 0.14	2.4	2.0	1.98 ± 0.18	
	$\eta' \omega$	0.01 ± 0.00	0.04	0.02	...	
	$\eta \phi$	0.16 ± 0.02	0.19	0.18	0.167 ± 0.034	
$\eta \rho^0$	0.59 ± 0.07	0.54	0.45	...		
$\eta' \rho^0$	0.06 ± 0.01	0.21	0.27	...		
D^+	$\pi^+ \rho^0$	0.61 ± 0.10	0.42	0.58	0.83 ± 0.15	
	$\pi^0 \rho^+$	4.53 ± 0.64	2.7	2.5	...	
	$\pi^+ \omega$	0.26 ± 0.07	0.95	0.80	0.28 ± 0.06	
	$\pi^+ \phi$	6.29 ± 0.20	5.65	5.65	5.68 ± 0.11	
	$\eta \rho^+$	1.02 ± 0.34	0.7	2.2	...	
	$\eta' \rho^+$	1.03 ± 0.11	0.7	0.8	...	
	$K^+ \bar{K}^{*0}$	3.82 ± 0.25	3.61	3.60	$3.83^{+0.14}_{-0.21}$	
	$\bar{K}^0 K^{*+}$	9.80 ± 0.41	11	11	34 ± 16	
	D_s^+	$\pi^+ K^{*0}$	3.65 ± 0.24	2.52	2.35	2.13 ± 0.36
		$\pi^0 K^{*+}$	1.02 ± 0.07	0.8	1.0	...
		$K^+ \rho^0$	2.10 ± 0.10	1.9	2.5	2.5 ± 0.4
		$K^0 \rho^+$	11.47 ± 0.48	9.1	9.6	...
ηK^{*+}		0.64 ± 0.20	0.2	0.2	...	
$\eta' K^{*+}$		0.33 ± 0.02	0.2	0.2	...	
$K^+ \omega$		2.12 ± 0.10	0.6	0.07	0.87 ± 0.25	
$K^+ \phi$		0.12 ± 0.02	0.166	0.166	0.182 ± 0.041	

that the predicted branching fraction of 0.6 before $\rho - \omega$ mixing agrees with the data of 0.87 ± 0.25 [67], while the predicted value of 0.07 after the mixing effect is far too small. Therefore, irrespective of $\rho - \omega$ mixing, $D^0 \rightarrow \pi^0 \omega$ and $D_s^+ \rightarrow K^+ \omega$ cannot be explained simultaneously in the FAT or modified FAT approach.

C. Direct CP violation

It has been noticed that weak penguin annihilation will receive sizable long-distance contributions from final-state rescattering. We shall assume that the long-distance PE_V and PE_P are of the same order of magnitude as E_V and E_P

TABLE IX. Same as Table VIII except for the direct CP asymmetries of $D \rightarrow VP$ decays in units of 10^{-3} , where $a_{\text{dir}}^{(\text{tree})}$ denotes CP asymmetry arising from purely tree amplitudes. The superscript (t + p) denotes tree plus QCD-penguin amplitudes, (t + pa) for tree plus weak penguin-annihilation (PE and PA) amplitudes and “tot” for the total amplitude.

Mode	$a_{\text{dir}}^{(\text{tree})}$	$a_{\text{dir}}^{(\text{t+p})}$	$a_{\text{dir}}^{(\text{t+pa})}$	$a_{\text{dir}}^{(\text{tot})}$ (this work)	$a_{\text{dir}}^{(\text{tot})}$ [69]	
D^0	$\pi^+\rho^-$	0	0.01 ± 0.00	0.76 ± 0.22	0.77 ± 0.22	-0.03
	$\pi^-\rho^+$	0	-0.09 ± 0.01	-0.05 ± 0.04	-0.14 ± 0.04	-0.01
	$\pi^0\rho^0$	0	-0.03 ± 0.00	0.40 ± 0.15	0.37 ± 0.15	-0.03
	K^+K^{*-}	0	-0.19 ± 0.01	-0.56 ± 0.37	-0.75 ± 0.37	-0.01
	K^-K^{*+}	0	0.11 ± 0.01	0.05 ± 0.04	0.15 ± 0.04	0
	$K^0\bar{K}^{*0}$	-0.15 ± 0.21	-0.15 ± 0.21	-0.15 ± 0.21	-0.15 ± 0.21	-0.7
	\bar{K}^0K^{*0}	-0.34 ± 0.16	-0.34 ± 0.16	-0.34 ± 0.16	-0.34 ± 0.16	-0.7
	$\pi^0\omega$	0	0.18 ± 0.04	-2.31 ± 0.96	-2.14 ± 0.95	0.02
	$\pi^0\phi$	0	0	0	0	-0.0002
	$\eta\omega$	-0.10 ± 0.01	-0.08 ± 0.01	-0.40 ± 0.10	-0.38 ± 0.10	-0.1
	$\eta'\omega$	2.40 ± 0.34	1.91 ± 0.25	1.42 ± 0.71	0.96 ± 0.66	2.2
	$\eta\phi$	0	0	0	0	0.003
	$\eta\rho^0$	0.39 ± 0.05	0.59 ± 0.08	-0.10 ± 0.29	0.10 ± 0.30	1.0
	$\eta'\rho^0$	-0.55 ± 0.07	-0.51 ± 0.07	0.12 ± 0.22	0.16 ± 0.22	-0.1
	D^+	$\pi^+\rho^0$	0	1.44 ± 0.11	0.78 ± 1.30	2.20 ± 1.38
$\pi^0\rho^+$		0	-0.40 ± 0.03	0.90 ± 0.37	0.49 ± 0.37	0.2
$\pi^+\omega$		0	-0.13 ± 0.03	0.84 ± 2.05	0.74 ± 2.03	-0.05
$\pi^+\phi$		0	0	0	0	-0.0001
$\eta\rho^+$		1.55 ± 0.26	2.12 ± 0.36	1.22 ± 0.65	1.78 ± 0.69	-0.6
$\eta'\rho^+$		-0.25 ± 0.05	-0.24 ± 0.04	0.10 ± 0.12	0.08 ± 0.11	0.5
$K^+\bar{K}^{*0}$		-0.14 ± 0.02	-0.27 ± 0.02	-0.94 ± 0.30	-1.06 ± 0.30	0.2
\bar{K}^0K^{*+}		-0.06 ± 0.01	0.06 ± 0.01	-0.01 ± 0.04	0.10 ± 0.04	0.04
D_s^+	π^+K^{*0}	0.14 ± 0.02	0.24 ± 0.02	0.94 ± 0.30	1.05 ± 0.30	-0.1
	π^0K^{*+}	0.10 ± 0.03	0.04 ± 0.04	1.21 ± 0.39	1.15 ± 0.40	-0.2
	$K^+\rho^0$	0.10 ± 0.02	-0.02 ± 0.02	0.03 ± 0.07	-0.08 ± 0.07	0.3
	$K^0\rho^+$	0.06 ± 0.01	-0.03 ± 0.01	0.01 ± 0.04	-0.08 ± 0.04	0.3
	ηK^{*+}	-1.03 ± 0.17	-0.33 ± 0.06	-0.61 ± 0.47	0.10 ± 0.48	1.1
	$\eta'K^{*+}$	0.25 ± 0.04	0.24 ± 0.03	-0.11 ± 0.14	-0.12 ± 0.13	-0.5
	$K^+\omega$	-0.09 ± 0.02	-0.03 ± 0.02	-0.05 ± 0.07	0.01 ± 0.08	-2.3
	$K^+\phi$	0	0	0	0	-0.8

in Solution (S6), respectively. For concreteness, we take (in units of 10^{-6})

$$(PE_V)^{\text{LD}} \approx (0.26 \pm 0.05)e^{i(224 \pm 30)^\circ},$$

$$(PE_P)^{\text{LD}} \approx (1.66 \pm 0.33)e^{-i(108 \pm 30)^\circ}. \quad (64)$$

The calculated results are shown in Table IX. In comparison, the predictions given in [69] in general are substantially smaller than ours in magnitude. We find several golden modes for the search of CP violation in the VP sector:

$$D^0 \rightarrow \pi^+\rho^-, K^+K^{*-}, \quad D^+ \rightarrow K^+\bar{K}^{*0}, \eta\rho^+,$$

$$D_s^+ \rightarrow \pi^+K^{*0}, \pi^0K^{*+}. \quad (65)$$

These modes are “golden” in the sense that they have large branching fractions and sizable CP asymmetries of order

1×10^{-3} . It is interesting to notice that the CP asymmetry difference defined by

$$\Delta A_{CP}^{VP} \equiv a_{CP}(K^+K^{*-}) - a_{CP}(\pi^+\rho^-), \quad (66)$$

in analogy to ΔA_{CP}^{PP} defined in Eq. (1), is predicted to be $(-1.52 \pm 0.43) \times 10^{-3}$, which is very similar to the recently observed CP violation in $D^0 \rightarrow K^+K^-$ and $D^0 \rightarrow \pi^+\pi^-$. It is thus desirable to first search for CP violation in the aforementioned golden modes.

V. DISCUSSIONS AND CONCLUSIONS

In this analysis, we have revisited two-body hadronic charmed meson decays to PP and VP final states, where P and V denote light pseudoscalar and vector mesons, respectively. Taking flavor $SU(3)$ symmetry as our working assumption for the Cabibbo-favored decays, we extract

tree-type flavor amplitudes through a global fit to the latest experimental data. We then discuss whether and how SU(3) symmetry breaking factors should be taken into account when moving on to the singly Cabibbo-suppressed decay modes. We have made predictions for the branching fractions as well as the CP asymmetries for these decay modes where we observe that the importance of penguin-type amplitudes, if present, often significantly modify the latter.

In the PP sector, several SU(3) breaking effects are crucial in explaining the measured branching fractions of singly Cabibbo-suppressed decay modes, as already noticed in Ref. [37]. The T and C amplitudes should be scaled by a factor given under the factorization assumption. We acknowledge that the E amplitude is governed mainly by long-distance rescattering effects and, therefore, the associated symmetry breaking factors need to be obtained via a fit to the four D^0 decays. In particular, one has to distinguish between two types of W -exchange amplitudes: E_d and E_s , depending upon whether it is $d\bar{d}$ or $s\bar{s}$ pair coming out of the exchange diagram. While $|E_d|$ is about 10% larger in magnitude than $|E|$ of the Cabibbo-favored modes, $|E_s|$ has two possibilities: either larger or smaller than $|E|$ by about 40%, as given in Eq. (16). The above-mentioned SU(3) symmetry breaking effects are most notably successful in explaining the large disparity between $\mathcal{B}(D^0 \rightarrow \pi^+\pi^-)$ and $\mathcal{B}(D^0 \rightarrow K^+K^-)$.

To test among different theory models, we have proposed to have a better precision in the measurement of $a_{CP}(D^0 \rightarrow K_S K_S)$, which is primarily due to interference between E_d and E_s amplitudes. We also revisit the CP asymmetry difference between $D^0 \rightarrow K^+K^-$ and $D^0 \rightarrow \pi^+\pi^-$ and find two results: $\Delta a_{CP}^{\text{dir}} = (-1.14 \pm 0.26) \times 10^{-3}$ for Solution I and $(-1.25 \pm 0.25) \times 10^{-3}$ for Solution II. Both of them are consistent with the latest LHCb result [29] within 1σ . We have also observed that these predictions are sensitive to the assumed contribution from weak penguin annihilation diagrams. Comparisons with a few other works are made to highlight the distinctive features of our approach.

In contrast to the PP sector, a global fit to the Cabibbo-favored modes in the VP sector gives many solutions with similarly small local minima in χ^2 (six of them, as listed in Table IV, when we restrict ourselves to $\chi_{\text{min}}^2 < 10$), revealing significant degeneracy in the current data. These solutions can explain the Cabibbo-favored decay branching fractions well except for the $D_s^+ \rightarrow \bar{K}^0 K^{*+}$ and $\rho^+ \eta'$

modes. For the former, we urge the experimental colleagues to update the figure. For the latter, an amplitude sum rule confines its branching fraction in the range (1.6,3.9)% at the 1σ level.

The above-mentioned solution degeneracy is lifted once we use them to predict for the singly Cabibbo-suppressed modes. In the end, we find that only Solutions (S3) and (S6) which have a common feature that C_V and C_P are close in phase in order to simultaneously explain the small $\mathcal{B}(D^0 \rightarrow \pi^0 \omega)$ and large $\mathcal{B}(D^0 \rightarrow \pi^0 \rho^0)$. Another common feature is that A_V and A_P are comparable in size and similar in phase, in order to simultaneously explain the small $\mathcal{B}(D^+ \rightarrow \pi^+ \omega)$ and large $\mathcal{B}(D^+ \rightarrow \pi^+ \rho^0)$. We note that the recent BESIII result of $\mathcal{B}(D_s^+ \rightarrow K^+ \omega)$ is a factor of 2 to 3 smaller than our prediction, and remains an issue to be resolved.

Unlike the PP sector, the singly Cabibbo-suppressed decay data in the VP sector do not call for an introduction of SU(3) breaking for the $T_{V,P}$ and $C_{V,P}$ amplitudes dictated by the factorization assumption. Instead, SU(3) breaking in $E_{V,P}$ is still required and, analogous to the PP sector, one should consider different long-distance effects on diagrams with $d\bar{d}$ and $s\bar{s}$ emerging from the W exchange. A fit to eight singly Cabibbo-suppressed D^0 decays shows that the symmetry breaking effects are often large. We have identified the set with the smallest SU(3) breaking in the E -type amplitudes ($< 50\%$) of Solution (S6) as our best solution and make predictions for the branching fractions and CP asymmetries of the singly Cabibbo-suppressed decays. In particular, we point out that the $D^0 \rightarrow \pi^+ \rho^-$, $K^+ K^{*-}$, $D^+ \rightarrow K^+ \bar{K}^{*0}$, $\eta \rho^+$, and $D_s^+ \rightarrow \pi^+ K^{*0}$, $\pi^0 K^{*+}$ modes have sufficiently large branching fractions and CP asymmetries at per mille level. Interestingly, $\Delta a_{CP}^{VP} \equiv a_{CP}(K^+ K^{*-}) - a_{CP}(\pi^+ \rho^-) \simeq (-1.52 \pm 0.43) \times 10^{-3}$, very similar to the recently observed CP violation in $D^0 \rightarrow K^+ K^-$ and $D^0 \rightarrow \pi^+ \pi^-$.

ACKNOWLEDGMENTS

This research was supported in part by the Ministry of Science and Technology of R.O.C. under Grants No. MOST-107-2119-M-001-034, No. MOST-104-2628-M-002-014-MY4 and No. MOST-108-2112-M-002-005-MY3. C. W. C. is grateful to the Mainz Institute for Theoretical Physics (MITP) of the DFG Cluster of Excellence PRISMA⁺ (Project ID 39083149) for its hospitality and its partial support during the completion of this work.

[1] R. Aaij *et al.* (LHCb Collaboration), *Phys. Rev. Lett.* **108**, 111602 (2012).

[2] G. Isidori, J. F. Kamenik, Z. Ligeti, and G. Perez, *Phys. Lett. B* **711**, 46 (2012).

- [3] K. Wang and G. Zhu, *Phys. Lett. B* **709**, 362 (2012).
- [4] A. N. Rozanov and M. I. Vysotsky, *JETP Lett.* **95**, 397 (2012).
- [5] Y. Hochberg and Y. Nir, *Phys. Rev. Lett.* **108**, 261601 (2012).
- [6] X. Chang, M. K. Du, C. Liu, J. S. Lu, and S. Yang, [arXiv:1201.2565](https://arxiv.org/abs/1201.2565).
- [7] G. F. Giudice, G. Isidori, and P. Paradisi, *J. High Energy Phys.* **04** (2012) 060.
- [8] W. Altmannshofer, R. Primulando, C. T. Yu, and F. Yu, *J. High Energy Phys.* **04** (2012) 049.
- [9] C. H. Chen, C. Q. Geng, and W. Wang, *Phys. Rev. D* **85**, 077702 (2012).
- [10] G. Hiller, Y. Hochberg, and Y. Nir, *Phys. Rev. D* **85**, 116008 (2012).
- [11] Y. Grossman, A. L. Kagan, and J. Zupan, *Phys. Rev. D* **85**, 114036 (2012).
- [12] C. H. Chen, C. Q. Geng, and W. Wang, *Phys. Lett. B* **718**, 946 (2013).
- [13] C. Delaunay, J. F. Kamenik, G. Perez, and L. Randall, *J. High Energy Phys.* **01** (2013) 027.
- [14] L. Da Rold, C. Delaunay, C. Grojean, and G. Perez, *J. High Energy Phys.* **02** (2013) 149.
- [15] D. Delepine, G. Faisel, and C. A. Ramirez, *Phys. Rev. D* **87**, 075017 (2013).
- [16] J. Brod, A. L. Kagan, and J. Zupan, *Phys. Rev. D* **86**, 014023 (2012).
- [17] D. Pirtskhalava and P. Uttayarat, *Phys. Lett. B* **712**, 81 (2012).
- [18] B. Bhattacharya, M. Gronau, and J. L. Rosner, *Phys. Rev. D* **85**, 054014 (2012).
- [19] T. Feldmann, S. Nandi, and A. Soni, *J. High Energy Phys.* **06** (2012) 007.
- [20] E. Franco, S. Mishima, and L. Silvestrini, *J. High Energy Phys.* **05** (2012) 140.
- [21] J. Brod, Y. Grossman, A. L. Kagan, and J. Zupan, *J. High Energy Phys.* **10** (2012) 161.
- [22] D. Atwood and A. Soni, *Prog. Theor. Exp. Phys.* **2013**, 093B05 (2013).
- [23] G. Hiller, M. Jung, and S. Schacht, *Phys. Rev. D* **87**, 014024 (2013).
- [24] T. Aaltonen *et al.* (CDF Collaboration), *Phys. Rev. Lett.* **109**, 111801 (2012).
- [25] B. R. Ko (Belle Collaboration), *Proc. Sci.*, ICHEP2012 (2013) 353 [[arXiv:1212.1975](https://arxiv.org/abs/1212.1975)].
- [26] R. Aaij *et al.* (LHCb Collaboration), *Phys. Lett. B* **723**, 33 (2013).
- [27] R. Aaij *et al.* (LHCb Collaboration), *J. High Energy Phys.* **07** (2014) 041.
- [28] R. Aaij *et al.* (LHCb Collaboration), *Phys. Rev. Lett.* **116**, 191601 (2016).
- [29] R. Aaij *et al.* (LHCb Collaboration), *Phys. Rev. Lett.* **122**, 211803 (2019).
- [30] Z. Z. Xing, *Mod. Phys. Lett. A* **34**, 1950238 (2019).
- [31] M. Chala, A. Lenz, A. V. Rusov, and J. Scholtz, *J. High Energy Phys.* **07** (2019) 161.
- [32] H. N. Li, C. D. Lü, and F. S. Yu, [arXiv:1903.10638](https://arxiv.org/abs/1903.10638).
- [33] Y. Grossman and S. Schacht, *J. High Energy Phys.* **07** (2019) 020.
- [34] A. Soni, [arXiv:1905.00907](https://arxiv.org/abs/1905.00907).
- [35] A. Khodjamirian and A. A. Petrov, *Phys. Lett. B* **774**, 235 (2017).
- [36] H. Y. Cheng and C. W. Chiang, *Phys. Rev. D* **85**, 034036 (2012).
- [37] H. Y. Cheng and C. W. Chiang, *Phys. Rev. D* **86**, 014014 (2012).
- [38] Y. Amhis *et al.* (HFLAV Collaboration), *Eur. Phys. J. C* **77**, 895 (2017); and online update at <https://hflav.web.cern.ch>.
- [39] H.-N. Li, C. D. Lü, and F. S. Yu, *Phys. Rev. D* **86**, 036012 (2012).
- [40] B. Aubert *et al.* (BABAR Collaboration), *Phys. Rev. D* **79**, 032003 (2009).
- [41] H. Y. Cheng, C. W. Chiang, and A. L. Kuo, *Phys. Rev. D* **93**, 114010 (2016).
- [42] L. L. C. Wang, *AIP Conf. Proc.* **72**, 419 (1980); *Weak Interactions as Probes of Unification*, edited by G. B. Collins, L. N. Chang, and J. R. Ficenec, and in *Proceedings of the 1980 Guangzhou Conference on Theoretical Particle Physics* (Science Press, Beijing, China, 1980), distributed by Van Nostrand Reinhold Company, pp. 1218–1232; L. L. Chau, *Phys. Rep.* **95**, 1 (1983).
- [43] L. L. Chau and H. Y. Cheng, *Phys. Rev. Lett.* **56**, 1655 (1986).
- [44] L. L. Chau and H. Y. Cheng, *Phys. Rev. D* **36**, 137 (1987); *Phys. Lett. B* **222**, 285 (1989).
- [45] H. Y. Cheng and S. Oh, *J. High Energy Phys.* **09** (2011) 024.
- [46] M. Tanabashi *et al.* (Particle Data Group), *Phys. Rev. D* **98**, 030001 (2018), and 2019 update.
- [47] R. Aaij *et al.* (LHCb Collaboration), *J. High Energy Phys.* **01** (2015) 024.
- [48] H. Y. Cheng and C. W. Chiang, *Phys. Rev. D* **81**, 074021 (2010).
- [49] P. Żenczykowski, *Acta Phys. Pol. B* **28**, 1605 (1997).
- [50] H. Y. Cheng, *Eur. Phys. J. C* **26**, 551 (2003).
- [51] L. L. Chau and H. Y. Cheng, *Phys. Lett. B* **333**, 514 (1994).
- [52] D. Besson *et al.* (CLEO Collaboration), *Phys. Rev. D* **80**, 032005 (2009).
- [53] F. Buccella, A. Paul, and P. Santorelli, *Phys. Rev. D* **99**, 113001 (2019).
- [54] M. Beneke, G. Buchalla, M. Neubert, and C. T. Sachrajda, *Phys. Rev. Lett.* **83**, 1914 (1999); *Nucl. Phys.* **B591**, 313 (2000).
- [55] M. Beneke and M. Neubert, *Nucl. Phys.* **B675**, 333 (2003).
- [56] M. Wirbel, B. Stech, and M. Bauer, *Z. Phys. C* **29**, 637 (1985); M. Bauer, B. Stech, and M. Wirbel, *ibid.* **34**, 103 (1987).
- [57] L. L. Chau and H. Y. Cheng, *Phys. Rev. Lett.* **53**, 1037 (1984).
- [58] U. Nierste and S. Schacht, *Phys. Rev. D* **92**, 054036 (2015).
- [59] R. Aaij *et al.* (LHCb Collaboration), *J. High Energy Phys.* **10** (2015) 055.
- [60] R. Aaij *et al.* (LHCb Collaboration), *J. High Energy Phys.* **11** (2018) 048.
- [61] N. Dash *et al.* (Belle Collaboration), *Phys. Rev. Lett.* **119**, 171801 (2017).
- [62] J. Laiho, E. Lunghi, and R. S. Van de Water, *Phys. Rev. D* **81**, 034503 (2010); 2+1 Flavor QCD Averages: <http://mypage.iu.edu/~elunghi/webpage/LatAves/index.html>.
- [63] H. Y. Cheng and C. K. Chua, *Phys. Rev. D* **80**, 114008 (2009); **80**, 074031 (2009).

- [64] Y. L. Wu, M. Zhong, and Y. B. Zuo, *Int. J. Mod. Phys. A* **21**, 6125 (2006).
- [65] H. Y. Cheng and C. K. Chua, *Phys. Rev. D* **80**, 114008 (2009).
- [66] W. Y. Chen *et al.* (CLEO Collaboration), *Phys. Lett. B* **226**, 192 (1989).
- [67] M. Ablikim *et al.* (BESIII Collaboration), *Phys. Rev. D* **99**, 091101 (2019).
- [68] M. Ablikim *et al.* (BESIII Collaboration), *Phys. Lett. B* **798**, 135017 (2019).
- [69] Q. Qin, H. N. Li, C. D. Lü, and F. S. Yu, *Phys. Rev. D* **89**, 054006 (2014).